

UPSLOPE WALKING WITH TRANSFEMORAL PROSTHESIS USING
OPTIMIZATION BASED SPLINE GENERATION

A Thesis
by
VICTOR CHRISTIAN PAREDES CAUNA

Submitted to the Office of Graduate and Professional Studies of
Texas A&M University
in partial fulfillment of the requirements for the degree of
MASTER OF SCIENCE

Chair of Committee, Pilwon Hur
Committee Members, Bryan Rasmussen
Shuguang Cui

Head of Department, Andreas A. Polycarpou

May 2016

Major Subject: Mechanical Engineering

Copyright 2016 Victor Christian Paredes Cauna

ABSTRACT

Powered prosthetic devices are robotic systems that are aimed to restore the mobility of subjects with amputations above the knee by imitating the behavior of a normal human leg. Powered prosthesis have diverse advantages with respect to passive devices, such as the possibility to reduce the metabolic cost of the user and to provide net power into the walking gait, among other advantages. In particular, this thesis is focused on the capacity of powered transfemoral prosthesis to be adaptive for diverse terrains. Since most environments consist of flat and inclined surfaces, we propose a framework able to generate gaits for both. The new framework is based on the Human-Inspired control and a spline based trajectory generation. Particularly, the trajectory generation blends flat ground trajectories for the ankle and knee into upslope walking trajectories. The proposed method is based on the insertion of a set of cubic splines that hold conditions of smoothness along its path and also through the use of impedance control for terrain adaptation. This framework will be tested on the prosthetic device AMPRO II for upslope walking and for flat ground terrains to motivate its use as a nominal controller for a transfemoral prosthesis. Current control framework in AMPRO II is based on the direct tracking of the trajectories obtained after the human-inspired optimization. The main objective of the thesis is to propose a framework that enables flatground and upslope walking using the base framework of the human-inspired control and spline based trajectory generation.

DEDICATION

I wish to dedicate this work to my parents, without their support none of my academic formation would be possible. Struggles never stopped their love and support for me.

ACKNOWLEDGEMENTS

This work is motivated by my supportive and patient advisor Dr. Pilwon Hur, I want to acknowledge as well the opportunity to work in his lab and under his guidance. Also, I want to extend the acknowledgment to all the people in Hur group that generates a positive learning environment.

NOMENCLATURE

B/CS	Bryan/College Station
HSUS	Humane Society of the United States
P	Pressure
T	Time
TVA	Tennessee Valley Authority
TxDOT	Texas Department of Transportation
PD	Proportional and derivative
QP	Quadratic Program
MIQP	Model Independent QP
CLF	Control Lyapunov Function
CWF	Canonical walking functions
HZD	Hybrid Zero Dynamics
PHZD	Partial Hybrid Zero Dynamcics
PS	Prosthetic leg support
HS	Human leg support

TABLE OF CONTENTS

	Page
ABSTRACT	ii
DEDICATION	iii
ACKNOWLEDGEMENTS	iv
NOMENCLATURE	v
TABLE OF CONTENTS	vi
LIST OF FIGURES	viii
LIST OF TABLES	xi
1. INTRODUCTION	1
1.1 Upslope Walking	6
1.2 Convex optimization for upslope walking	8
1.3 AMPRO II	8
1.4 Thesis Structure	10
2. HUMAN UPSLOPE WALKING ANALYSIS	12
2.1 Bipedal locomotion	12
2.1.1 Kinematics of human walking	12
2.2 Upslope Walking Kinematics	15
2.3 Human Walking data	15
2.4 Strategies for walking upslope	17
2.4.1 Human Strategy	17
2.4.2 Controller Strategy	18
3. FLAT TERRAIN GAIT GENERATION	20
3.1 Bipedal Model	20
3.2 Human-inspired control	24
3.2.1 Canonical walking functions	24
3.2.2 Human-Inspired Outputs	26
3.2.3 Control design	27

3.2.4	Partial Hybrid Zero Dynamics	28
3.3	Human-inspired optimization	29
3.4	Motion capture system	30
3.5	Simulation of the flat ground gait	33
3.6	Gait generation for non flat terrain	34
3.6.1	Extended canonical walking functions for rough terrain	34
3.6.2	Upstairs walking	35
3.6.3	Limitations	35
4.	OPTIMIZATION-BASED SPLINE GENERATION FOR UPSLOPE WALKING	37
4.1	Problem Formulation	37
4.2	Analytical solution	43
4.3	Human-inspired walking with cubic splines	44
4.3.1	Trajectories generated	46
4.4	Implementation details	46
5.	RESULTS	48
5.1	Flat ground walking	49
5.1.1	HIC results	50
5.1.2	SHIC results	51
5.2	Upslope walking	51
5.3	Controllers comparison	51
5.3.1	Flat ground walking using HIC and SHIC	52
5.3.2	Flat ground and upslope walking using SHIC	53
5.4	SHIC control action	53
6.	CONCLUSIONS	58
	REFERENCES	59

LIST OF FIGURES

FIGURE	Page
1.1 Ottobock 3R60 EBS knee joint with a prosthetic foot. This passive prosthesis is controlled through an hydraulic system adapted to the damping requirements of human walking.	3
1.2 Ottobock's C-Leg is a microprocessor controlled Knee. This powered prosthesis is controlled through an hydraulic system with controlled damping.	3
1.3 The Vanderbilt prosthesis is an ankle and knee powered device. It was developed in Vanderbilt University by the Center of Intelligent Mechatronics.	4
1.4 AMPRO 1 is a powered trans-femoral prosthesis based on electrical motors and Human-Inspired control.	6
1.5 AMPRO 2 is a second generation of the prosthetic devices at Texas A&M. Each component is shown on one of the three views of the prosthesis.	9
1.6 IMU placement on the subject. The IMUs are used to interface with AMPRO II	9
2.1 Illustration of the phases of human walking under the assumption of flat foot walking. During double support phase both legs supports the weight contrary to single support phase where one the legs support the weight.	13
2.2 The ankle joint can move in two directions, to avoid ambiguity those directions are called dorsiflexion and plantar flexion. Regarding the knee the directions of rotation are called as flexion and extension. . . .	14
2.3 Ankle Trajectory for 0°, 5°, 8°and 10°slope inclinations. The data is taken from McIntosh [16].	16
2.4 Knee Trajectory for 0°, 5°, 8°and 10°slope inclinations. The data is taken from McIntosh [16].	16

2.5	Low gain PD action used to enable terrain adaptation.	18
2.6	Ankle and knee flat ground trajectories. The red shaded region represents the action of the splines and the blue shaded regions the action of the low PD control. The human data is taken from McIntosh [16].	19
3.1	Bipedal robotic model considering the same anthropomorphic dimensions as the human subject.	21
3.2	Human data collected though IMUs represented as canonical walking functions. They are conformed by the hip position (m) and the joints relations (rad).	25
3.3	Trajectories generated by the human-inspired optimization for ankle and knee.	31
3.4	Trajectories generated by the human-inspired optimization for ankle and knee.	32
3.5	Ankle and knee phase portrait, indicating a continuous evolution of the system and a discrete change in velocity at impact.	32
3.6	Canonical walking functions obtained in the simulation.	33
3.7	Gait tile simulation using feedback linearization control.	34
4.1	Two disconnected trajectories C_1 and C_2 can be connected trough a trajectory S , starting from time t_s and finishing on t_c	37
4.2	Connecting two different trajectories using a set of splines joined by specific waypoints	38
4.3	Cubic splines connected through waypoints	39
4.4	Trajectory generation for ankle and knee joint. The splines has been generated in two extremes to show the effect of the splines.	47
5.1	Healthy subject using a knee adapter to use the transfemoral prosthesis AMPRO II	48
5.2	Indoors flat ground walking experiment using SHIC.	49
5.3	Outdoors experiment using SHIC.	50
5.4	Ankle and knee Tracking for flat ground walking using HIC.	50

5.5	Ankle and knee Tracking for flat ground walking using SHIC.	51
5.6	Upslope walking trajectories for ankle and knee. The slope inclination is 13°.	52
5.7	Superposition of the trajectories for flat ground surfaces using both controllers, splines-based human-inspired control and normal human- inspired control	52
5.8	2-steps trajectory differences between flat ground and upslope walking using SHIC.	53
5.9	SHIC low gain PD (red region) and spline generation (blue region) for two steps.	54
5.10	Flat ground walking using SHIC.	55
5.11	Transition between flat ground walking to upslope walking using SHIC.	56
5.12	Upslope walking sequence using SHIC.	57

LIST OF TABLES

TABLE	Page
4.1 Implementation parameters	47

1. INTRODUCTION

Amputation can play a negative role in the development of the persons in different contexts affecting the access to some opportunities and even impacting on the depression levels on the persons [17]. In particular, lower limb amputations also imposes a big effect on the mobility, specifically walking gait. This motivates the development prostheses that can attenuate this problem by imitating the behavior of normal human legs, providing the possibility of recovering the damaged walking skills.

Lower limb amputations can be classified as amputations below the knee (trans-tibial) and above the knee (trans-femoral). Experiments suggest that trans-femoral amputees behave in a less active life style compared to trans-tibial amputees, particularly the maximum aerobic capacity was significantly lower in above the knee amputees compared to below the knee amputees [24]. This facts justify the study and development of trans-femoral devices to bypass the limitations of impaired subjects. Trans-femoral prostheses are expected to achieve a human-like walking and meet several requirements, such as, bear the user's body weight, be safe on its operational cycle, cooperate with the user and provide the possibility to traverse diverse terrains.

It is estimated that there are approximately 185,000 new amputations each year in United States [15]. Furthermore, according to a report by the National Center for Health Statistics it is estimated that from the 1.2 million people in the United States that lives with limb loss, 18.5 percent are trans-femoral amputees [21].

Despite the great development on feedback control, most of the available prostheses in the market are energetically passive devices, in other words, they do not con-

tribute to the insertion of net power during the walking cycle. Essentially they are mechanically actuated devices with passive elements such as spring and dampers. In consequence their mechanical behavior is fixed and the terrain they can traverse is limited. However, even with the exposed limitations of passive trans-femoral prosthesis, they are reliable devices that are lightweight and easy to use.

In recent years, several powered devices have been developed to overcome some of the weaknesses that passive prosthesis have. These weaknesses include, for instance, the lack of user's control over the prosthesis and the limited adaptation to different kind of terrains. The capacity to mimic human behaviors on powered trans-femoral prosthesis due to the active actuation over the joints. Basically a powered device is composed by ankle and knee actuators driven by a computer computing a feedback control algorithm designed to interact with the user and resemble the walking gait for different scenarios.

In particular, micro-controller-based knee devices are powered devices that only actuates over the knee. Usually the micro-controller changes the knee damping properties depending on the selected task it is performing. Available micro-controller based knees are increasing its presence in the market, such prostheses can be represented by the C-Leg4 (1.2) and the Ottobock's (Fig 1.1), among others.

Powered trans-femoral prosthesis with actuation in the ankle and knee offers the possibility to enhance the performance of the walking gait with respect to the knee actuated devices. Although it increases the complexity of the system, advances in feedback control allows to generate human-like gaits with on-board processing.



Figure 1.1: Ottobock 3R60 EBS knee joint with a prosthetic foot. This passive prosthesis is controlled through an hydraulic system adapted to the damping requirements of human walking.



Figure 1.2: Ottobock's C-Leg is a microprocessor controlled Knee. This powered prosthesis is controlled through an hydraulic system with controlled damping.

In the research community one of the most representatives full powered (ankle and knee) prosthesis was developed by Vanderbilt [22, 11], this prosthesis is an electrically actuated device based on impedance control [8] by using set of impedance parameters along its walking cycle, the impedance is modeled as a linear spring and a damper. The gait cycle is decomposed in several phases as the gait progresses. Each phase is represented by their unique set of impedance parameters and is selected through a state machine. The parameters defining the impedance functions must be tuned based on joint sensor data, video recordings and user feedback [22]. The Vanderbilt prosthesis is shown in Fig. 1.3. Note that this framework depends on a tuning process to acquire the impedance parameters for each subject, this characteristic limits its practical implementation for a massive number of users.

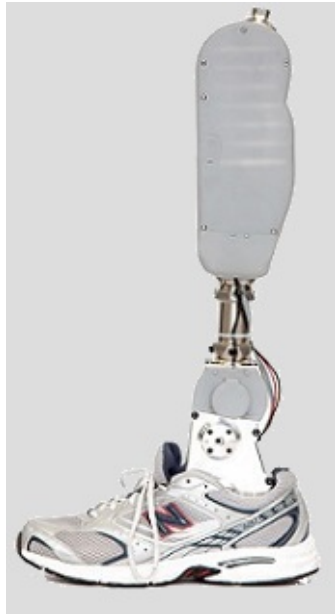


Figure 1.3: The Vanderbilt prosthesis is an ankle and knee powered device. It was developed in Vanderbilt University by the Center of Intelligent Mechatronics.

An important result that avoids to perform a tuning process since it allows to automatically generate stable and human-like walking gaits is given by the human-inspired control [2, 1]. It is a control framework based on Hybrid Zero Dynamics (HZD) [27, 26]. This framework was originally formulated toward bipedal robots, it uses the mathematical descriptions of the impacts modeled as a discrete event together with of the continuous dynamics through the use of hybrid systems [20]. In particular, the human-Inspired control [1, 2] is based on a human-inspired optimization (HIO) which generates output functions that given that a suitable controller tracks them, it renders the robotic system stable and hybrid invariant. Human-inspired control has successfully been implemented in bipedal robots such as AMBER I [28], AMBER II [30], DURUS [7] and ATRIAS [6].

This control framework has also been extended for powered trans-femoral prosthesis and tested in the prosthetic device AMPRO I [33] (Fig. 1.4), the first generation of trans-femoral prosthesis developed at Texas A&M University by AMBER Lab (now at Georgia Tech). Two different assumptions on the walking gait can be considered under the human-inspired control, i) a flat foot, single-contact behavior [33], which captures the essentials of human walking and ii) a multi-contact behavior which expands the results on the flat foot assumption and that generates a more human-like walking gait [31]. Note that the assumption of flat foot walking is useful for testing new algorithms since it provides a simple framework for implementation. After a successfully implementation of an algorithm it can be translated into the framework considering multi-contact walking gaits. Note that is reported that the knee behavior generated with flat foot walking shows a similar trajectory with respect to the human knee, but a different ankle trajectory with respect to the human ankle [33]. However, this situation is improved by using multi-contact walking gaits because they include more phases of the human walking cycle [31].

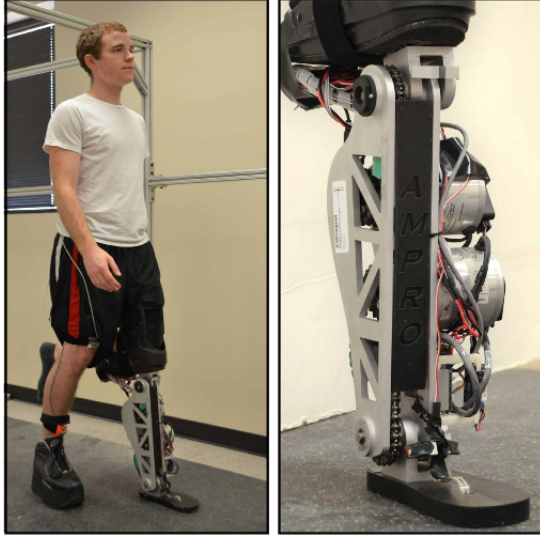


Figure 1.4: AMPRO 1 is a powered trans-femoral prosthesis based on electrical motors and Human-Inspired control.

1.1 Upslope Walking

As mentioned earlier, an important characteristic required for prosthesis is the capacity to traverse diverse terrains. In order to achieve this in a powered trans-femoral prosthesis it is important to construct controllers able to traverse common terrains that can be found during walking such as rough terrain, stairs and ramps. Since flat ground and sloped surfaces are very common for most environments. In particular, this thesis focuses on the generation of walking gaits able to generate flat ground and upslope walking gaits.

Most research effort has been placed in flat ground terrain walking generation [5, 33, 22], however, [23] extended the previous flat ground algorithm based on impedance control to work with inclined surfaces. The algorithm involves a tuning process to get the impedance parameters for two different inclinations of 5° and 10° . During

walking when an inclined surface is detected its inclination is estimated by the prosthesis and the closest inclination from the database (5° and 10°) is chosen as the set of parameters used for the gait. Increasing the number of inclinations to cover a broader spectrum of inclinations would become infeasible, because of the tuning process it would require.

As indicated, the human-inspired walking can automatically generate stable and human-like walking gaits for trans-femoral prosthesis, bypassing the tuning process. Although, there is not an implementation of an upslope algorithm, a stair walking ascending algorithm [29] was proposed and tested for AMPRO I. This algorithm is based on *a priori* information about the stairs profile (each step height and width), this information is used in the HIO for the generation of a walking gait for that specific surface. Note that due to the computational effort the HIO must be computed offline.

Furthermore, information about the terrain cannot be obtained for most situations, it means that running the HIO is not practical for real environments that includes a variety of different surfaces. This limitation of the human-inspired walking motivates the usage of more flexible schemes. However, diIt is beneficial to keep the advantages of human-inspired control, specially the automatically generation of walking gaits. To generate upslope walking trajectories for the ankle and knee joints of a prosthesis without the burden of using the HIO for every slope, it is possible to look at convex optimization formulations since they have fast solutions that can be performed in real time. The generation of trajectories based on the use of a convex optimization formulation has been utilized for generation task-space trajectories into legged robotics [10] through the use of cubic splines.

1.2 Convex optimization for upslope walking

It can be observed that sloped surfaces are traversed with ease by humans, studying the kinematics underlying the human movements during upslope walking and comparing them with flat ground walking gaits gives directions about the qualitative strategies used by humans when traversing this kind of terrains. The main idea is the generation of upslope walking trajectories by blending nominal flat ground walking gaits using the strategies found by looking at human data.

Considering biomechanics studies for inclined surfaces, [16] found that the knee seems to be sensitive enough to differentiate the surface inclination angle, from those results it can be observed that the ankle and knee present some trends on its evolution with respect to the flat ground walking gait. These trends will be analyzed for the generation of strategies in the prosthetic device.

1.3 AMPRO II

AMPRO (A&M Prosthetic) II is the second version of the AMPRO prosthesis series that are custom designed and built at Texas A&M University by AMBER Lab (now at Georgia Tech). Compared to the first generation of AMPRO [33], the main improvements of the second version are three folds: a) the weight is reduced to $5kg$, which is more than $3kg$ weight reduction; b) the height is reduced by $71mm$ and the width is reduced by $36mm$. The smaller size will allow a wider height range of subjects to be able to use this device; c) the motors and electronics are placed higher up on the calf resulting a higher center of mass position, which yields a much more smaller inertial for the device. Additionally, two FlexiForce force sensors are mounted on the heel and toe for contact detection and leg switch. The main code structure including the online gait generation code is running on a low-power single core micro computer BeagleBone Black at $200Hz$. Details of the design diagram

can be seen in Fig. 1.5. In order to interface with AMPRO II, the human leg is instrumented with two IMUs located at the shin and thigh (Fig. 1.6).

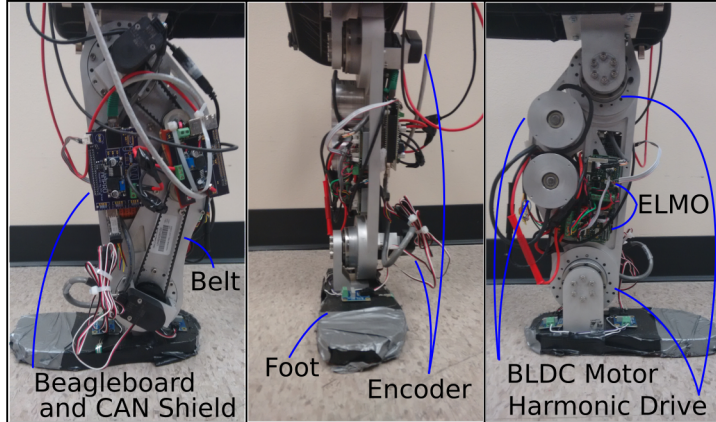


Figure 1.5: AMPRO 2 is a second generation of the prosthetic devices at Texas A&M. Each component is shown on one of the three views of the prosthesis.

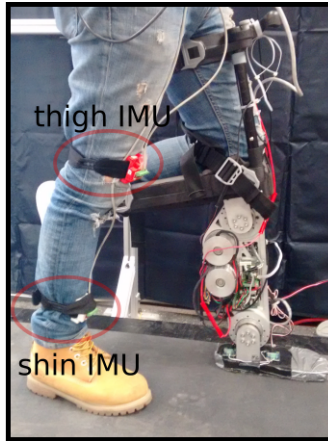


Figure 1.6: IMU placement on the subject. The IMUs are used to interface with AMPRO II

The high level controller, the human-inspired control, is computed on the embedded BeagleBone, which takes as inputs the values from the encoders, the FlexiForce sensors and the IMUs data. The desired torques are commanded to the ELMO drives through CANopen communication, then each ELMO drive implements a low-level joint controller to deliver the desired torque at their respective joints. To process the IMU data, another BeagleBone is used to compute an extended Kalman filter (EKF) which estimates the human hip position, used as a parameterization of time for the human-inspired control.

1.4 Thesis Structure

The flow of the thesis will be briefly discussed in this section. Chapter 2 presents basic definitions of the human walking and a summary of the human-inspired controller along with some discussion about its advantages and limitations in the context of upslope walking.

In Chapter 3, the kinematics underlying upslope walking will be studied to characterize the strategies followed by healthy humans when they are traversing inclined surfaces. By comparing ankle and knee trajectories from flat ground to upslope walking it is possible to draw important conclusions in the way humans blend the flat ground trajectories into upslope trajectories.

The optimization formulation for the cubic splines is explained and constructed in Chapter 4, this formulation is based on the analysis of the strategies followed to realize upslope walking. Particularly, it presents a convex-optimization formulation aimed to replicate those strategies. This chapter also shows the modification of canonical walking functions to take consideration of the generated splines.

The results of the application of the splines with the human-inspired control are shown in Chapter 5. The blended trajectories designed using the spline formulation

are shown and explained for different scenarios. The implementation and data acquisition was conducted using the prosthetic device AMPRO II.

The conclusions are presented in Chapter 6, a comparison is made between the standard walking controller for flat ground terrain and the splines based controller. The idea is to motivate the usage of the spline based controller as a general framework to traverse different surfaces within the same framework. Additionally open problems and improvements are discussed for guiding new research on this topic.

2. HUMAN UPSLOPE WALKING ANALYSIS

This chapter presents an overview of the human data analysis for flat ground and upslope walking gaits. In particular, by analyzing the kinematic data of healthy humans during upslope walking it is possible to extract high level strategies used to motivate the main formulation: blending flat ground trajectories into upslope walking gaits.

2.1 Bipedal locomotion

Bipedal locomotion is a highly non-linear process, since several muscles can contribute during a single movement of a limb, the analysis of the dynamics and forces involved during human walking can be complex. Given the difference in dynamics between the human leg and a transfemoral prosthesis, it is not possible to find a simple correspondence between forces, instead a kinematic relation can be used to capture the high-level human behavior.

2.1.1 Kinematics of human walking

Human walking can be studied in the light of the kinematics despite the differences in dynamics between a robotic model and an actual human. To study kinematics of human walking it is important to distinguish between the basic walking phases that are involved in the walking cycle: *single support phase* and *double support phase*. During single support phase (2.1) the leg supporting the human body weight is called *stance leg* and the leg going forward is the *swing leg*. Furthermore, in the context of prostheses, it is useful to differentiate between the human leg and the prosthetic leg, for instance, it is useful to use human stance leg or prosthesis stance leg to differentiate between possibilities.

To motivate the previous definitions, a description of normal walking cycle will be discussed. During walking, there is a cyclic process on the movement of the legs: starting in double support phase (2.1) both legs are supporting the human body weight, then one of the legs become stance leg and the other swing leg. The swing legs moves to its desired location until it impacts the ground, entering again to the double support phase, swapping the naming of the legs (stance leg and swing leg) and finalizing one step. . Note that for the scope of the thesis, flat foot walking is being imposed on the walking gait and behaviors such as heel strike or toe push are left for future work.

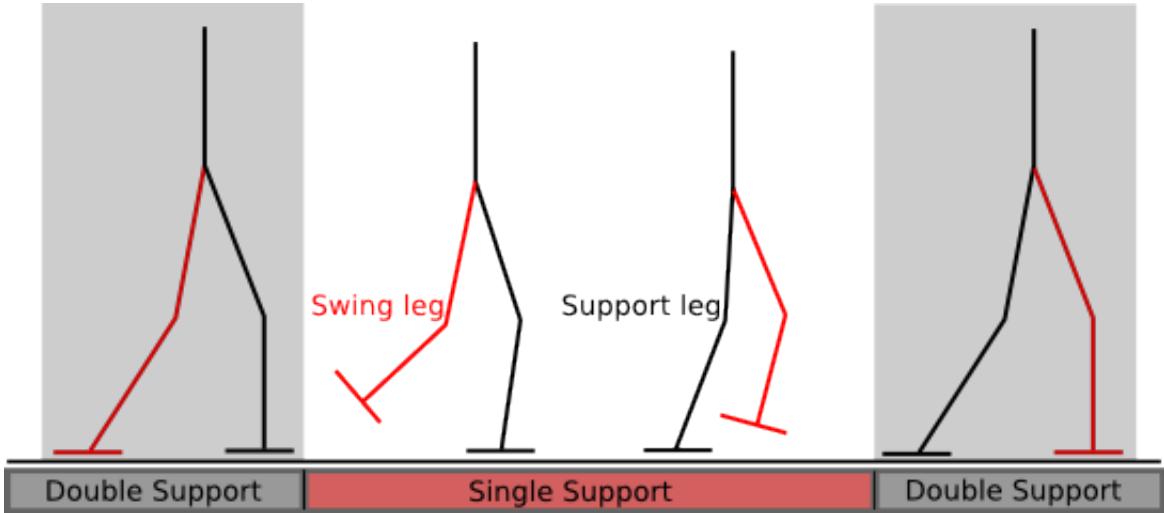


Figure 2.1: Illustration of the phases of human walking under the assumption of flat foot walking. During double support phase both legs supports the weight contrary to single support phase where one the legs support the weight.

Also, the knee and ankle movements can be described by their direction of movement, particularly flexion and extension plays an important role to identify clearly

the direction of movement of a joint. For ankle, dorsiflexion happens when the foot rotates around the ankle toward the leg and plantarflexion otherwise (Fig. 2.2). In the case of the knee, extension happens when this rotation makes the leg move forward and Knee flexion otherwise (Fig. 2.2).

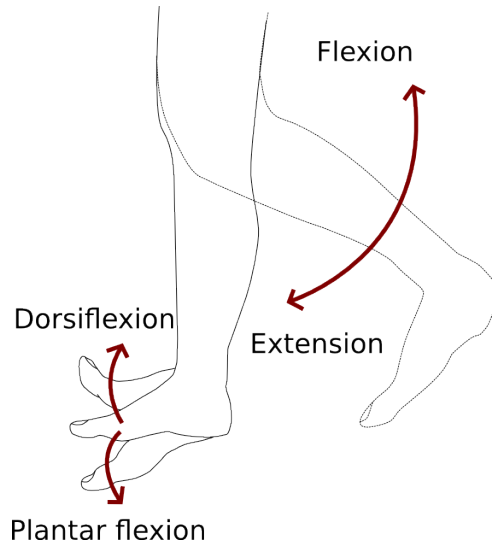


Figure 2.2: The ankle joint can move in two directions, to avoid ambiguity those directions are called dorsiflexion and plantar flexion. Regarding the knee the directions of rotation are called as flexion and extension.

This subsection has described important terminology to reference rotational movements of the lower limbs that will be useful for future references in the thesis. The next subsection will explore the kinematics involving upslope walking in healthy humans.

2.2 Upslope Walking Kinematics

Inclined surfaces are often present during locomotion activities, pedestrians walk on this kind of surfaces frequently in the streets, buildings and other environments. In consequence upslope walking is an important desired terrain that needs to be traversed by transfemoral prosthesis. As a first step for the design of upslope walking gaits, it is to look at human data to gather important conclusions.

A great amount of study has focused primarily on flat ground walking [16], studying the changes in the kinematics pattern with respect to flat ground walking when humans perform upslope walking may expose some inherent behavior that can provide insight into the control strategies used [12] by humans to traverse inclined surfaces. Those strategies could be captured and implemented into prosthetic devices from a suitable nominal flat ground walking gait.

2.3 Human Walking data

Motivated by the studies in inclined surface walking [16, 12, 14], it is shown that the knee flexion increases as the inclination of the surface increases. In particular the knee trajectory for different surfaces (Fig. 2.4) indicated a consistent trend on the trajectory changes with respect to slope increase. The same trend with, although with less variation, is present in the ankle trajectories (Fig. 2.3). This increase for both joints are explained partially on the geometry of the surface because it makes the ankle dorsiflexion and knee flexion to increase in order to avoid foot scuffing with the surface.

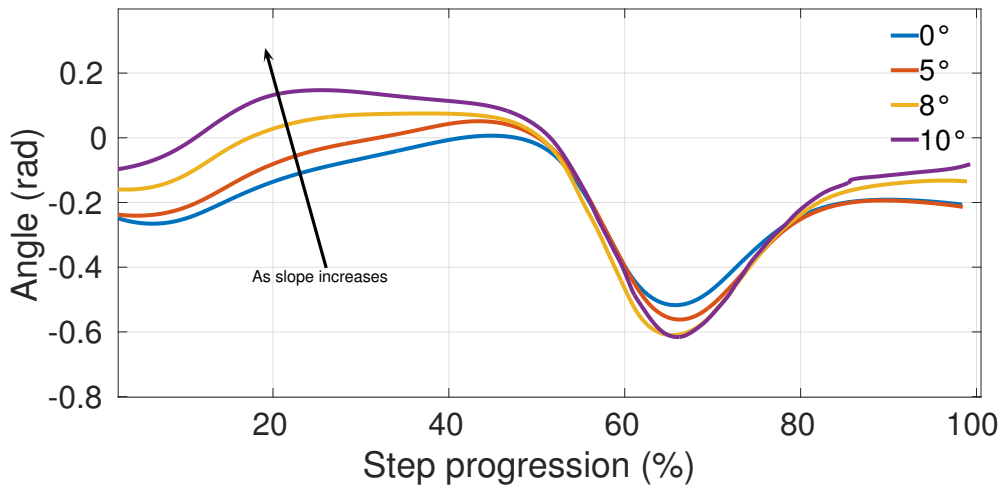


Figure 2.3: Ankle Trajectory for 0° , 5° , 8° and 10° slope inclinations. The data is taken from McIntosh [16].

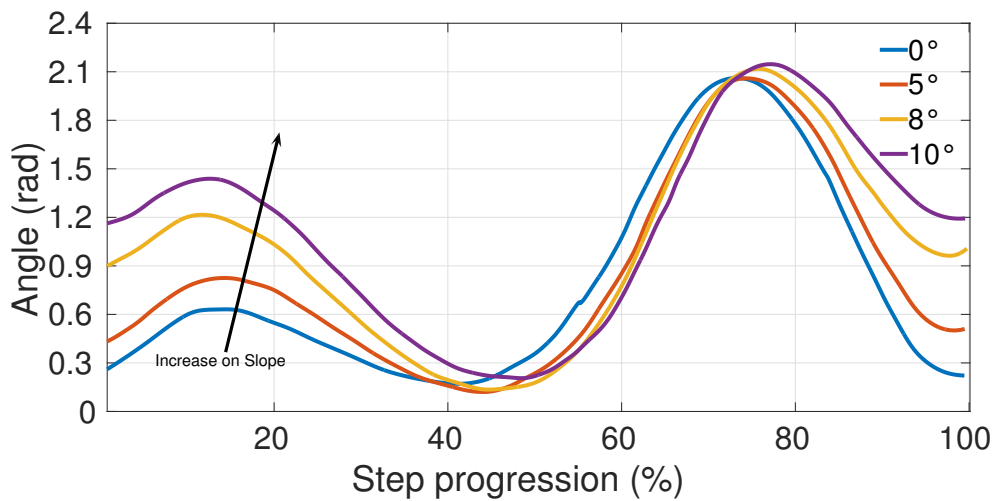


Figure 2.4: Knee Trajectory for 0° , 5° , 8° and 10° slope inclinations. The data is taken from McIntosh [16].

2.4 Strategies for walking upslope

The trajectories for ankle and knee (Fig. 2.3 and Fig. 2.4) shows that most of the variation on trajectories is present in the extremes of the trajectories, in other words, at the beginning of stance phase and at the final part of the swing phase. In the next subsections a brief discussion about the human strategies used during upslope walking will be used to motivate the blending of flat ground walking into upslope walking in the context of a transfemoral prosthesis.

2.4.1 Human Strategy

Although it is possible to describe upslope walking with all the rigor involving the dynamics [16], focusing on the kinematic trends allows to develop high-level strategies to 'mimic' the behavior of humans during upslope walking independently of the dynamics differences between a human leg and the prosthetic leg. The first values of ankle and knee (Fig. 2.3 and Fig. 2.4) are imposed by the inclined surface, in other words, the geometry of the slope modifies the angular values of the ankle and knee. As the slope increases the ankle will have greater dorsiflexion and the knee will have greater flexion. Those results are consistent with [16], which reports that knee flexion at heel strike increase from 7° from 33° with an increase of surface inclination angle from 0° to $+10^\circ$. Note that knee is the most sensitive joint with respect to the slope inclination [16].

The differences in ankle and knee introduce with respect to the flat ground trajectories can be considered as a new initial condition into the system, it is observed that from this initial condition the trajectories converge into the nominal flat ground trajectories approximately at 40% of the step progression and evolves similarly to the flat ground walking gait until approximately 80% of the step progression, where the trajectories suffer deviations again because of the geometry of the surface.

2.4.2 Controller Strategy

A simple algorithm is proposed to blend flat ground into upslope walking trajectories. This algorithm is based in two simple actions: (1) generate in real time a trajectory that starts from the condition imposed by the surface (red shade region in Fig. 2.6) and (2) use low gain PD control that can offer terrain adaptation at the final part of the step (blue shaded region in Fig. 2.6). The low gain PD control can shape the angles of the joints at the final part of the step progression in order to let the prosthesis to acquire more knee flexion as the slope increases (Fig. 2.5).

In particular, as the generation of trajectories requires to be calculated in real time and to meet several constraints, such as smoothness and boundedness for physically admissible velocities and accelerations, the formulation takes the form of a convex optimization problem. The convex optimization formulation will be discussed later and merged into the human-inspired walking formulation to generate a complete framework that yields flat ground and upslope walking gaits.

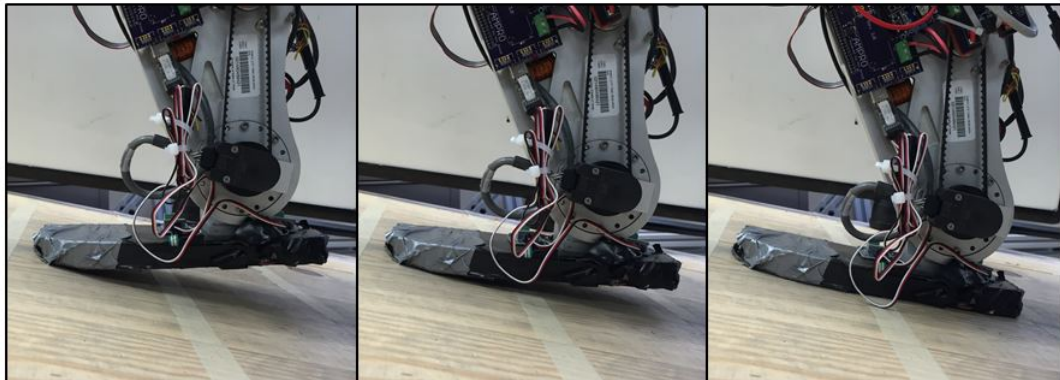


Figure 2.5: Low gain PD action used to enable terrain adaptation.

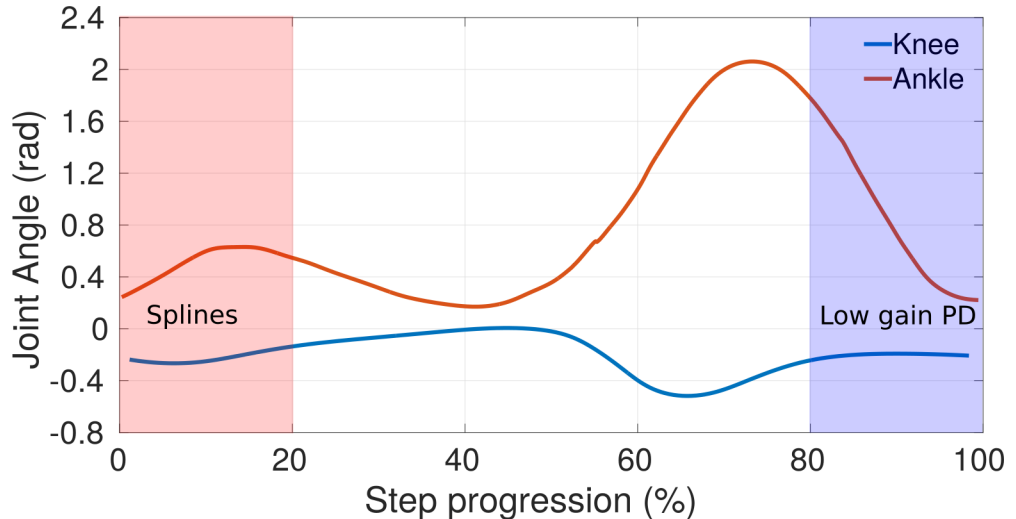


Figure 2.6: Ankle and knee flat ground trajectories. The red shaded region represents the action of the splines and the blue shaded regions the action of the low PD control. The human data is taken from McIntosh [16].

The low gain PD control on the ankle and knee act as a passive spring and damper with a fixed equilibrium, the parameters are chosen in this case to adapt to knee surfaces. The controller takes the following form:

$$\tau_i = kp_i(\theta_{actual,i} - \theta_{desired,i}) + kd_i(\dot{\theta}_{actual,i} - \dot{\theta}_{desired,i}), \quad i \in \{ankle, knee\} \quad (2.1)$$

where, k_i , θ_i and b_i are the stiffness, equilibrium point and damping parameters describing the impedance. Note that impedance control is implemented in the last part of the step progression, most of the time the human-inspired control will drive the joints.

3. FLAT TERRAIN GAIT GENERATION

The generation of upslope walking gaits starts from the construction of automatically stable and human-like flat ground trajectories using the human-inspired control approach. The human-inspired control [2, 1, 28] is a method based on the HZD approach [27, 26] that uses human-data as a reference for the construction of functions that represent the human walking through simple mathematical expressions. These functions are fully defined through a non-linear optimization problem that is used to guarantee stability and to consider physical constraints of the device. By tracking these functions by an appropriate use of feedback control, the system becomes stable and performs human-like walking in bipedal robots and transfemoral prostheses.

3.1 Bipedal Model

A planar bipedal robotic model with 7-link (one torso, two thighs, two calves and two feet) which shares similar anthropomorphic values as the human is constructed to have a representation of the human in the generation of the walking gait. Analogously, the coordinates are chosen based on the human subject (3.1) as $\theta = \begin{bmatrix} \theta_{sa} & \theta_{sk} & \theta_{sh} & \theta_{nsh} & \theta_{nsk} & \theta_{nsa} \end{bmatrix}^T \in Q_R$, where Q_R is the configuration space, a submanifold of \mathbb{R}^6 .

The walking gait will be generated with the additional assumption of flat foot walking. It is considered that flat foot walking captures the essential movements of the walking gait [33] and is used as the testbed for implementation on more human-like walking representation such as multi-contact walking (for modeling multi-contact behavior see [30]). Additionally, during human walking, the impact with the ground plays a relevant event on the system that changes instantly the joint velocities [26], in order to take in consideration this discrete event the bipedal model is regarded as

a hybrid system [4, 26].

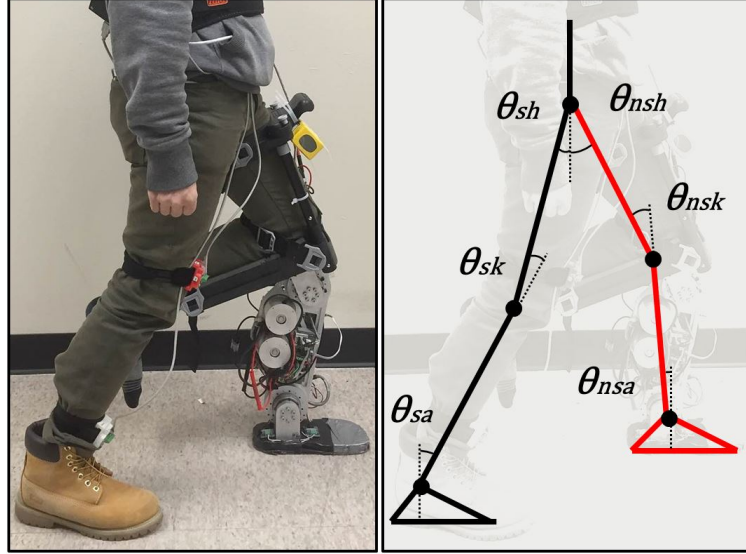


Figure 3.1: Bipedal robotic model considering the same anthropomorphic dimensions as the human subject.

The equations of motion representing the continuous dynamics of the system can be expressed as:

$$D(\theta)\ddot{\theta} + H(\theta, \dot{\theta}) = Bu \quad (3.1)$$

where, $D(\theta) \in \mathbb{R}^6$ is the inertial matrix and $H(\theta, \dot{\theta}) = C(\theta)\dot{\theta} + G(\theta)$, $C(\theta)$ the Coriolis term and $G(\theta)$ the gravity vector. Since we are assuming full actuation the torque map is the identity matrix, $B = I_6$. The input to the system is given by the torques u . Expressing (3.1) in terms of state space variable $x = (\theta, \dot{\theta})^T$, we found an affine

control system representation as shown below:

$$\dot{x} = f(x) + g(x)u \quad (3.2)$$

where,

$$f(x) = \begin{bmatrix} \dot{\theta} \\ -D^{-1}(\theta)H(\theta, \dot{\theta}) \end{bmatrix} \quad (3.3)$$

$$g(x) = \begin{bmatrix} 0 \\ D^{-1}(\theta)B(\theta) \end{bmatrix} \quad (3.4)$$

Definition 3.1.1. A hybrid control system is a tuple:

$$\mathcal{HC} = (X, U, S, \Delta, f, g) \quad (3.5)$$

where,

- X is a smooth submanifold of \mathbb{R}^6 .
- $U \subseteq \mathbb{R}^6$ is the space of admissible controls.
- $S \subsetneq X$ is the guard or switching surface.
- $\Delta : S \rightarrow X$ is the reset map.
- (f, g) is a control system s.t $\dot{x} = f(x) + g(x)u$.

To discriminate between single support phase and double support phase in the walking cycle, the unilateral constraint $h(\theta)$ is used. This constraint is the distance of the swing foot with respect to the ground, while this constraint is positive ($h(\theta) > 0$), it ensures that the swing foot is above the ground. An impact occurs when the

unilateral constraint becomes zero ($h(\theta) = 0$) and the velocity of impact is greater than zero ($\dot{h}(\theta) > 0$). Then the single support phase can be expressed as:

$$X = \{(\theta, \dot{\theta}) \in TQ_R : h(\theta) \geq 0\} \quad (3.6)$$

where, TQ_R is the tangent bundle of the system. The *guard* is defined as the boundary of the domain with the unilateral constraint decreasing, in other words, when the leg is impacting the ground with certain velocity. The guard can be expressed as:

$$S = \{(\theta, \dot{\theta}) \in TQ_R : h(\theta) = 0, \frac{dh(\theta)}{dt} > 0\} \quad (3.7)$$

To model the discrete event (impact), we assume that the impacts are plastic with impulsive forces acting on the system leg at the moment of contact. It is required to consider the extended coordinates that include the position of the support foot given by $\theta_e = (p_x, p_z, \theta)^T \in \mathbb{R}^2 \times Q_R$. Assume that the position of the swing foot end is defined as $\Gamma(\theta_e)$ and its Jacobian is given by $J_\Gamma(\theta_e)$. After an impact occurs the velocity of the joints suffers an instantaneous change in velocity, described by the *impact map*:

$$\dot{\theta}_e^+ = P(\theta_e)\dot{\theta}_e^- = (I - D^{-1}(\theta_e)J_\Gamma^T(\theta_e)(J_\Gamma(\theta_e)D^{-1}(\theta_e)J_\Gamma^T(\theta_e))^{-1}J_\Gamma(\theta_e))\dot{\theta}_e^- \quad (3.8)$$

Note that the joint positions does not change after the impact [26].

Whenever impacts occur the legs must be swapped, i.e, the support leg must be relabeled as the swing leg while the swing leg must be relabeled as the support leg. This is possible to achieve by the use of a coordinate transformation \mathfrak{R} . This

transformation is included in the *reset map* Δ .

$$\Delta : S \rightarrow X, \quad \Delta(\theta, \dot{\theta}) = \begin{bmatrix} \Re & 0 \\ 0 & \Re \end{bmatrix} \begin{bmatrix} \theta \\ P(\theta)\dot{\theta} \end{bmatrix} \quad (3.9)$$

In order to consider both the continuous dynamics and the discrete event the model was constructed as a hybrid control system (3.5).

3.2 Human-inspired control

With the appropriate model of the bipedal robotic system correlated with the human user, the next step towards the control design is the selection of control objectives. The idea is the tracking of functions that capture the behavior of human walking, these functions are the canonical walking functions, they are canonical in the sense that they are intrinsic in human walking. By tracking the canonical walking functions a robotic model can exhibit the same behavior as human walking despite the difference in dynamics [1, 20].

3.2.1 Canonical walking functions

The canonical walking functions are inherent to human walking, Ames [1] conducted experiments with several subjects, they exhibited the same evolution of some specific joint combinations, called as canonical walking functions. Considering the 7-link bipedal robot and the flat foot assumption a total of 6 canonical walking functions are required (Fig. 3.2), δp_{hip} the linearized hip position, θ_{sk} the supporting knee, θ_{nsk} the non-supporting knee, δm_{nsl} the non-supporting slope, θ_{torso} the torso angle and θ_{nsf} the non-supporting foot.

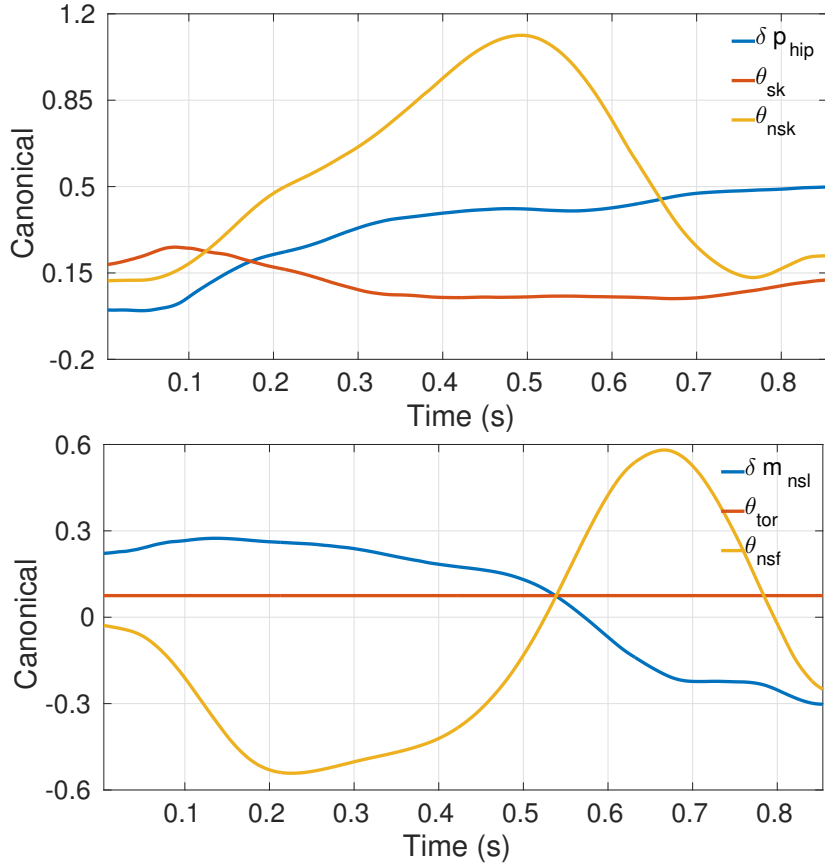


Figure 3.2: Human data collected though IMUs represented as canonical walking functions. They are conformed by the hip position (m) and the joints relations (rad).

The canonical walking functions have two different types of outputs, one of them corresponds to the linearized velocity of the hip ($y_1^d(\theta, \dot{\theta})$) and the rest can be modeled as the solution of a second order system ($y_2^d(\theta, \dot{\theta})$).

$$y_1^d(\theta, \dot{\theta}) = \delta \dot{p}_{\text{hip}}(\theta, \dot{\theta}) \quad (3.10)$$

$$y_2^d(\theta, \dot{\theta}) = \left[\theta_{\text{sk}}, \theta_{\text{nsk}}, \delta m_{\text{nsl}}, \theta_{\text{tor}}, \theta_{\text{nsf}} \right]^T \quad (3.11)$$

In general, each output $y_d(t, \alpha)$ can be described as functions dependent on a set of parameters α . Note that v_{hip} is considered to be a member of α

$$y_d^1(t) = v_{hip}t \quad (3.12)$$

$$y_{d,i}^2(t, \alpha) = e^{-\alpha_4 t} (\alpha_1 \cos(\alpha_2 t) + \alpha_3 \sin(\alpha_2 t)) + \alpha_5 \quad (3.13)$$

where, $i \in \{\theta_{sk}, \dot{\theta}_{sk}, \theta_{nsk}, \delta m_{nsl}, \theta_{torso}, \theta_{nsf}\}$.

3.2.2 Human-Inspired Outputs

The human inspired outputs are the tracking errors between the actual and desired canonical walking functions. By driving them to zero ($y(\theta, \dot{\theta}, \alpha) \rightarrow 0$), the robotic model will perform a human-like walking gait.

$$y(\theta, \dot{\theta}, \alpha) = \begin{bmatrix} y_1(\theta, \dot{\theta}) \\ y_2(\theta, \alpha) \end{bmatrix} = \begin{bmatrix} y_1^a(\theta, \dot{\theta}) - v_{hip} \\ y_2^a(\theta) - y_2^d(\rho(\theta), \alpha) \end{bmatrix} \quad (3.14)$$

Note that $y_1(\theta, \dot{\theta})$ is a relative degree one output and $y_2(\theta, \alpha)$ corresponds to the relative degree two outputs [19]. $\rho(\theta)$ is used as a parameterization of time based on the observation that the hip position is regarded to increase linearly on time [1]. The parameterization is given as:

$$\rho(\theta) = \frac{\delta_{p_{hip}}^+(\theta) - \delta_{p_{hip}}^+}{v_{hip}} \quad (3.15)$$

where, $\delta_{p_{hip}}^+(\theta)$ is the position of the hip at the beginning of the step, designed in the human-inspired optimization, described in the next section and $\delta_{p_{hip}}^+(\theta)$ is the actual (linearized) position of the hip. The importance of the parameterization of time is that using $\rho(\theta)$ as a phase variable the user have control over the progression of

the step, independent of time. The interaction between the user and the prosthesis makes it specially well suited for transfemoral prosthesis. The calculation of the phase variable $\rho(\theta)$ depends on which leg the user is supporting his or her weight. If the user is standing on the prosthesis leg, then the encoders are used to calculate ρ , otherwise, the IMUs attached to the healthy leg are used to estimate through a EKF the actual hip position [33].

3.2.3 Control design

Considering the human-inspired outputs defined in (3.14) the idea is to drive these outputs to zero. Applying the feedback linearization control [19] to the outputs, the resulting control law is:

$$\begin{bmatrix} \dot{y}_1 \\ \ddot{y}_2 \end{bmatrix} = \underbrace{\begin{bmatrix} L_{fy_1}(\theta, \dot{\theta}) \\ L_{fy_2}^2(\theta, \dot{\theta}, \alpha) \end{bmatrix}}_{L_f(\theta, \dot{\theta}, \alpha)} + \underbrace{\begin{bmatrix} L_{gy_1}(\theta, \dot{\theta}) \\ L_g L_{fy_2}(\theta, \dot{\theta}, \alpha) \end{bmatrix}}_{\mathcal{A}(\theta, \dot{\theta}, \alpha)} u \quad (3.16)$$

where, $L_f(\theta, \dot{\theta}, \alpha)$ represents the lie derivatives and $\mathcal{A}(\theta, \dot{\theta}, \alpha)$ is the decoupling matrix, which is invertible due to the selection of the outputs [32, 1].

Choosing a control a control input $u \in \mathcal{U}$ in the form $u = \mathcal{A}^{-1}(\theta, \dot{\theta}, \alpha)(L_f(\theta, \dot{\theta}, \alpha) + \mu$, the equation (3.14) becomes:

$$\begin{bmatrix} \dot{y}_1 \\ \ddot{y}_2 \end{bmatrix} = \mu \quad (3.17)$$

Note that for the bipedal model, exact information about the dynamics can be obtained, this allows to simulate the system and observe the resulting walking gait. However, for implementation purposes the dynamics of the user are unknown, thus the implementation of the controller needs to be model independent such as PD

control or Model Indepedent QP [33].

To drive the outputs to zero the form that μ take can be designed as:

$$\mu = \begin{bmatrix} -2\epsilon y_1 \\ -2\epsilon L_{fy_2} - \epsilon^2 y_2 \end{bmatrix} \quad (3.18)$$

3.2.4 Partial Hybrid Zero Dynamics

When the tracking outputs are driven to zero, the control law renders the Hybrid Zero Dynamics (HZD) surface:

$$Z_\alpha = \{(\theta, \dot{\theta}) \in TQ_R : y_1(\theta, \dot{\theta}) = 0, y_2(\theta, \alpha) = 0, L_{fy_2}(\theta, \dot{\theta}, \alpha) = 0\} \quad (3.19)$$

This surface describes an invariant set for the continuous dynamics, once the tracking objectives are driven to zero, then the outputs will stay at zero for posterior times, however it is desired to guarantee that the outputs are impact invariant as well. The dependence of the surface with the parameter α allows the search of canonical walking functions that can render the surface hybrid invariant [27]. Additionally, a less restrictive surface that allows changes in the hip velocity ($y_1^d = v_{hip}$) after the impact, might help to compensate to impulsive effect of impacts and the modeling errors, this surface is the Partial Hybrid Zero Dynamics (PHZD).

$$PZ_\alpha = \{(\theta, \dot{\theta}) \in TQ_R : y_2(\theta, \alpha) = 0, L_{fy_2}(\theta, \dot{\theta}, \alpha) = 0\} \quad (3.20)$$

The impacts on the system affects the joint velocities (3.8), this can deviate the system evolution away from the PHZD. In order to constrain the system to be invariant under impacts it is necessary to ensure that when the system is in the

switching surface S evolving in the PHZD surface, an impact Δ does not move the system away from the PHZD surface PZ_α . The PZHD constraint can be stated as:

$$\Delta(S \cap PZ_\alpha) = PZ_\alpha \quad (3.21)$$

Therefore, the goal is to select the parameters α such that the system renders the PHZD invariant under impacts [27, 1]. This can be enforced as a constraint in the human-inspired optimization.

3.3 Human-inspired optimization

The PHZD constraint generates human-like walking gaits that are provably stable [1, 28, 30]. Additionally more constraints must be imposed considering the limitations of the prosthesis, such as torque, position and velocity limits. All the requirements of the walking gait must be specified in the optimization problem along with the physical limitations of the device itself.

$$\begin{aligned} \alpha^* &= \underset{\alpha \in \mathbb{R}^{26}}{\operatorname{argmin}} \quad Cost_{HD}(\alpha) \\ \Delta(S \cap PZ_\alpha) &= PZ_\alpha \quad (3.22) \\ &\quad (\text{Physical constraints}) \end{aligned}$$

The cost function $Cost_{HD}(\alpha)$ is the square weighted square error between human data and the CWF, as shown in the expression below, the complete details of the optimization can be found in [1].

$$Cost_{HD}(\alpha) = \sum_{k=1}^K [(\beta_{y_1}(y_1(t[k], v_{hip}) - y_1^H(k)))^2 + \sum_{j=1}^5 \beta_{y_{2,j}}(y_{2,j}(t[k], \alpha) - y_{2,j}^H(k))^2] \quad (3.23)$$

where, K is the total number of points taken during the motion capture, $y_1^H(k)$ is the vector of values corresponding to the hip position at index k . The relative degree two data is labeled as $y_{2,j}^H(k)$ beign the index j the selector of one of the five relative degree two functions. The weights β are defined as the difference between the maximum and the minimum value of the output data.

$$\beta_{y_1} = 1/(\max_k(y_1^H(k)) - \min_k(y_1^H(k))) \quad (3.24)$$

$$\beta_{y_{2,j}} = 1/(\max(y_{2,j}^H(k)) - \min(y_{2,j}^H(k))), \quad j \in [1, 5] \quad (3.25)$$

The solution of the human-inspired optimization is a walking gait that is provably stable and human-like due to the human data beign used. A Poincare analysis is carried out to guarantee stability ensuring that the eigenvalues are less than 1 [25, 18, 1].

The strength of the human-inspired optimization is the automatic generation of stable and human-like walking gaits that requires no parameter tuning or calibration. Additionally, a series of constraints are imposed so the system can evolve in a feasible manner inside the designed bounds [33].

3.4 Motion capture system

To acquire human data a IMU-based motion capture system was used. The IMUs consisted in seven MPU-9150 devices (tri-axis gyroscope and tri-axis accelerometer), they were placed in fixed places in the feet, calves, thighs and torso. A kinematic model is constructed in the sagital plane starting from the hip, with the assumption that the hip acceleration is negligible. During the data recording procedure, an EKF is utilized to estimate the joint trajectories, which will be used as the references for the prosthetic gait design.

The human data captured by the IMU-based motion system is utilized on the human-inspired optimization (Fig. 3.2), and particularly Fig. 3.3 shows the ankle and knee joints.

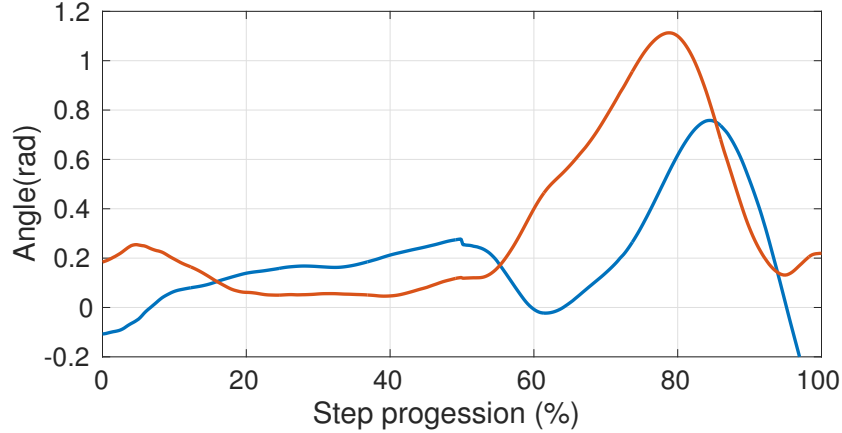


Figure 3.3: Trajectories generated by the human-inspired optimization for ankle and knee.

Note that the trajectories of the knee present differences with respect to normal human walking and it is because of the flat foot behavior requested to the subject. Solving the human-inspired optimization gives as a result the parameters α required to fully define the canonical walking functions. The ankle and knee trajectories generated for AMPRO II are shown in Fig. 3.4.

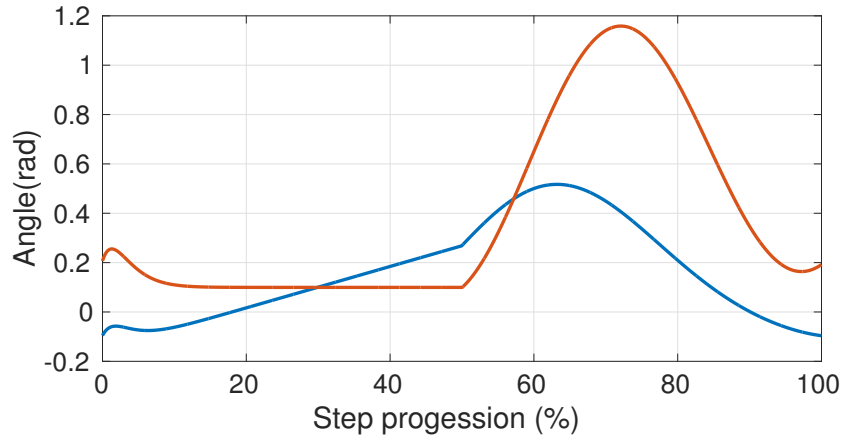


Figure 3.4: Trajectories generated by the human-inspired optimization for ankle and knee.

The phase portrait plot shown in Fig. 3.5 exhibits that the trajectories evolve into a continuous curve and then they are affected by a discrete impact (the discontinuity). Note that the discrete impact keeps the angle values but changes the joint velocities instantaneously (3.8).

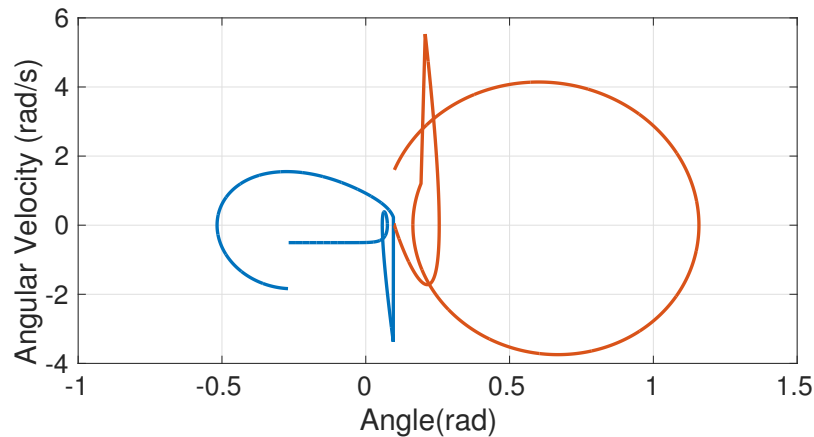


Figure 3.5: Ankle and knee phase portrait, indicating a continuous evolution of the system and a discrete change in velocity at impact.

3.5 Simulation of the flat ground gait

The simulation performed using feedback linearization generated an stable and human-like walking gait, represented in the walking tiles in Fig. 3.7.

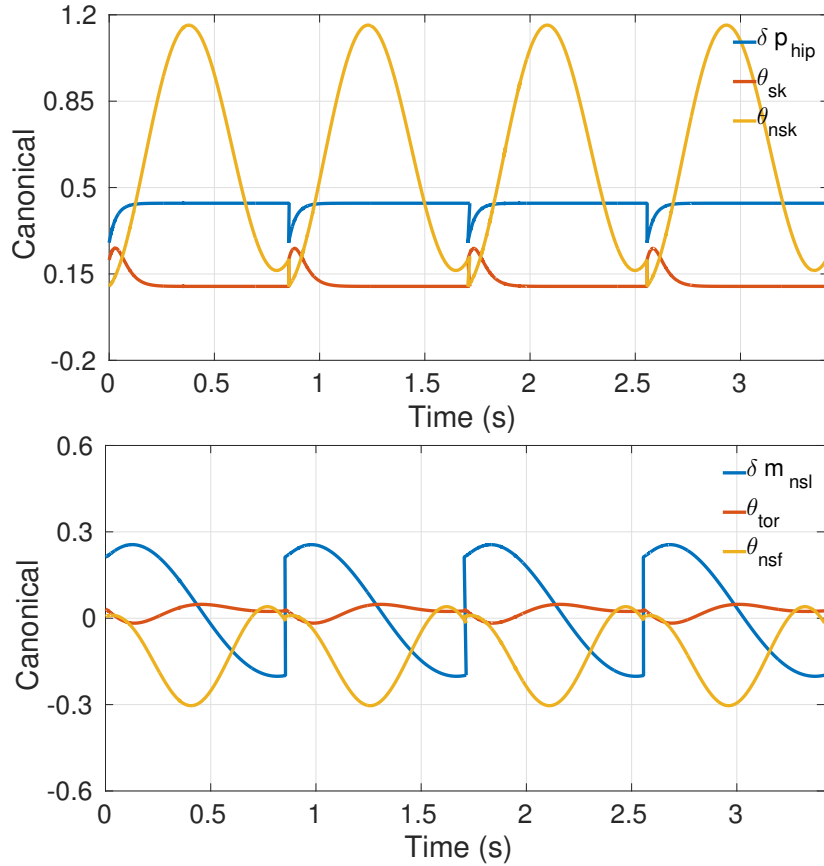


Figure 3.6: Canonical walking functions obtained in the simulation.

The canonical walking functions generated for this particular walking gait are shown in Fig. 3.6 for 4 steps. Note that hip velocity suffers a change after the impact but it converges to its desired value eventually.

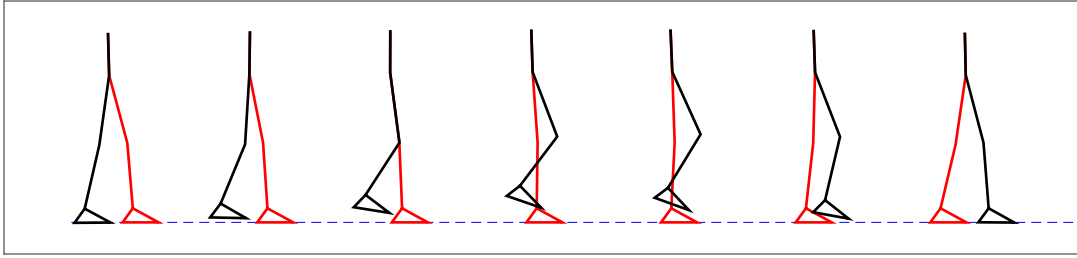


Figure 3.7: Gait tile simulation using feedback linearization control.

3.6 Gait generation for non flat terrain

The human-inspired control can be used to generate walking gaits for diverse terrain. This section will summarize the application of this framework for rough terrain and for stair ascending, additionally it presents a discussion about the limitations of the current framework and possible options to address adaptability for transfemoral prosthesis. Note that the summary of the additional methods is rather informal but references are provided for more details.

3.6.1 Extended canonical walking functions for rough terrain

Rough terrain imposes a challenge on the generation of human-inspired walking gaits due to the unknown and unpredictable terrain profile, Shishir [9] proposed that one solution to handle this problem is the modification of the CWF into the extended canonical walking functions (ECWF). The ECWF are constructed by the addition of more parameters that can be calculated in real time, depending on the initial conditions imposed by the surface.

$$y_2^e(t, \alpha) = e^{-\alpha_4 t} (\alpha_1 \cos(\alpha_2 t) + \alpha_3 \sin(\alpha_2 t)) + \alpha_5 \cos(\alpha_6 t) + \frac{2\alpha_5 \alpha_4 \alpha_2}{\alpha_2^2 + \alpha_4^2 - \alpha_6^2} \sin(\alpha_6 t) + \alpha_7 \quad (3.26)$$

Choosing the linear terms $\alpha_v = [\alpha_1, \alpha_3, \alpha_5, \alpha_7]$ we can construct a linear matrix equation by keeping $\alpha_2, \alpha_4, \alpha_6$ constant and solving the equation in order to accommodate the condition imposed by the surface [9]. In this manner, it allows freedom in the terrain profile by calculating a new α_v at every step.

3.6.2 Upstairs walking

The human-inspired optimization is highly dependent on the human-data and the terrain profile, using data for upstairs walking it would be possible to solve the human-inspired optimization given an appropriate redefinition of the guard S (3.7). In particular, the guard must define the terrain profile exactly in order to account for the impacts that happen during walking. Huihua et al. [29] generated a walking gait based on the human-inspired optimization given a priori knowledge of the stairs profile, the walking gait was implemented successfully into the prosthetic device AMPRO I.

3.6.3 Limitations

Note that in order to provide adaptability to new terrains it is important to generate joint trajectories that resemble the trajectories followed by healthy human subjects, for instance, while ECWF works for rough terrain, it cannot provide a specific desired behavior during upslope walking. Furthermore, if we are to use the human-inspired optimization for the generation of walking gaits at each new terrain, this problem could be unfeasible, as currently there is no solution on real time for this optimization. Additionally, in practical implementation with the prosthesis it is not possible to acquire information of the terrain profile.

In consequence, terrain adaptability requirements are twofold: i) Generation of trajectories with specific desired behaviors and ii) online solutions for the generation of new trajectories at every step. Regarding upslope walking, the generation of an

algorithm that holds the two conditions for terrain adaptability takes the form of a convex optimization formulation. The reason for choosing a convex optimization problem is because it is fast to solve and can be subject to constraints and objectives that can be formulated to mimic the behavior of upslope walking.

The next chapter will introduce the convex optimization problem that is aimed to the blending of the flat ground trajectories already generated into upslope walking by mimicking the qualitative strategies found in Chapter 2.

4. OPTIMIZATION-BASED SPLINE GENERATION FOR UPSLOPE WALKING

This chapter is motivated by the strategies found in human walking during upslope walking. A convex optimization based cubic spline problem is proposed due to its flexibility to be shaped into a desired behavior or trajectories and for the possibility to introduce constraints into the system that can be solved in real-time [10, 3]. Furthermore, an analytical solution is proposed that can be solved easily with most linear algebra packages in the microcomputer used in the prosthesis.

4.1 Problem Formulation

The generation of a trajectory S connecting a point (say, a point from trajectory C_1) to a nominal trajectory (say, trajectory C_2) as can be seen in Fig. 4.1 is the main goal of this chapter.

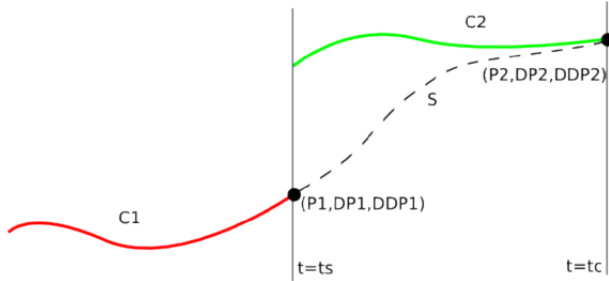


Figure 4.1: Two disconnected trajectories C_1 and C_2 can be connected through a trajectory S , starting from time t_s and finishing on t_c

Additionally, some important constraints must be met such as continuity in the

connection points with $C1$ and $C2$ and smoothness on the entire trajectory. A discontinuity in position would impose high velocities that can affect the performance of the walking gait, analogously a discontinuity in velocities can impose large accelerations.

A well-known solution to this problem is using a single cubic spline to connect the desired points. Cubic splines have four tunable parameters which can take care of continuity of position and velocity. Unfortunately it lacks the capability to provide smooth accelerations at the extreme points, also this single cubic spline cannot be shaped to follow a desired qualitative behavior (by fitting a trajectory). This solution can be improved using several intermediate points (waypoints) connecting cubic splines between the origin and destination points. This technique is more advantageous as continuity, smoothness and obstacle avoidance could be achieved by picking appropriate spline parameters [10]. The usage of waypoints and a set of splines (Fig. 4.2) can be exploited to define a cost function that allows to shape the behavior of the set of cubic splines by minimizing the distance to some reference curve.

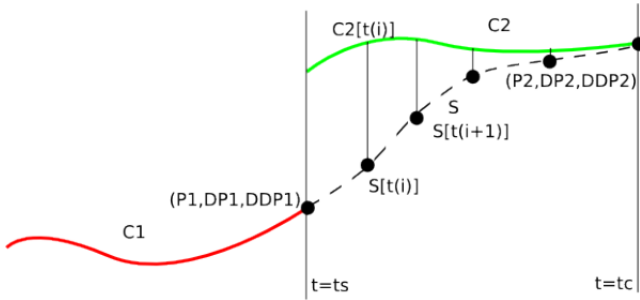


Figure 4.2: Connecting two different trajectories using a set of splines joined by specific waypoints

To guarantee that position, velocity and acceleration are smooth, it is necessary to check the waypoints. Each waypoint (except the extreme points) connects two splines. Both connected splines should have the same values in position, velocity and acceleration at each waypoint (Fig. 4.3).

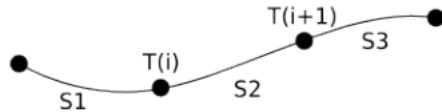


Figure 4.3: Cubic splines connected through waypoints

Assuming that the set of N splines S_1, S_2, \dots, S_N is represented by S , which is defined appropriately such that for a corresponding time t it takes the value of the corresponding spline $S_k(t), k \in [1, N]$. Particularly at the waypoints the time is defined by $T(i)$ for $i \in [1, N]$. The mathematical representation for smoothness in position, velocity and acceleration can be written as:

$$\begin{aligned} S_1(T(i)) &= S_2(T(i)) \\ \dot{S}_1(T(i)) &= \dot{S}_2(T(i)) \\ \ddot{S}_1(T(i)) &= \ddot{S}_2(T(i)) \end{aligned} \tag{4.1}$$

Since the objective is to generate a convergent trajectory that follows a desired behavior, it is necessary to have a cost function based on the distance between a reference trajectory and the generated splines, Fig. 4.2 shows the distance between each waypoint to the desired trajectory. These distances will be used for the construction

of the cost function, which is minimized through a least square formulation:

$$\min \sum_i ||S(T(i)) - C2(T(i))|| \quad (4.2)$$

$$s.t. \quad (4.1)$$

(Smoothness constraints)

In order to describe the smoothness conditions, assume that each cubic spline has the following form:

$$S_i = a_0^i + a_1^i(t - t_c) + a_2^i(t - t_c)^2 + a_3^i(t - t_c)^3 \quad (4.3)$$

where, $\lambda_i = \{a_0^i, a_1^i, a_2^i, a_3^i\}$ is the set of parameters that defines the spline, note that t_c is the convergence time (Fig. 4.1) and t_s is the switching time. To include conditions of smoothness for velocity and acceleration, it is necessary to calculate the derivatives and double derivatives of the cubic spline.

$$\dot{S}_i = a_1^i + 2a_2^i(t - t_c) + 3a_3^i(t - t_c)^2 \quad (4.4)$$

$$\ddot{S}_i = 2a_2^i + 6a_3^i(t - t_c) \quad (4.5)$$

To make the splines S_i and S_{i+1} to be continuous and smooth in terms of position, velocity and acceleration, its values at the waypoints should be equal. In the case of position, the conditions of smoothness are expressed as:

$$S_i(t_i) = a_0^i + a_1^i(\Delta_{t_i}) + a_2^i(\Delta_{t_i})^2 + a_3^i(\Delta_{t_i})^3 \quad (4.6)$$

$$S_{i+1}(t_i) = a_0^{i+1} + a_1^{i+1}(\Delta_{t_i}) + a_2^{i+1}(\Delta_{t_i})^2 + a_3^{i+1}(\Delta_{t_i})^3 \quad (4.7)$$

$$S_i(t_i) - S_{i+1}(t_i) = 0 \quad (4.8)$$

Considering smoothness in velocity, the conditions are expressed as:

$$\dot{S}_i(t_i) = a_1^i + 2a_2^i(\Delta_{t_i}) + 3a_3^i(\Delta_{t_i})^2 \quad (4.9)$$

$$\dot{S}_{i+1}(t_i) = a_1^{i+1} + 2a_2^{i+1}(\Delta_{t_i}) + 3a_3^{i+1}(\Delta_{t_i})^2 \quad (4.10)$$

$$\dot{S}_i(t_i) - \dot{S}_{i+1}(t_i) = 0 \quad (4.11)$$

Analogously for the smoothness conditions in acceleration:

$$\ddot{S}_i(t_i) = 2a_2^i + 6a_3^i(\Delta_{t_i}) \quad (4.12)$$

$$\ddot{S}_{i+1}(t_i) = 2a_2^{i+1} + 6a_3^{i+1}(\Delta_{t_i}) \quad (4.13)$$

$$\ddot{S}_i(t_i) - \ddot{S}_{i+1}(t_i) = 0 \quad (4.14)$$

These constraints can be written in matricial form. Consider a vector λ storing all the parameters of the splines, a segment of the vector $\lambda_{i,i+1}$ is constructed in the following way:

$$\lambda_{i,i+1} = \begin{bmatrix} a_0^i & a_1^i & a_2^i & a_3^i & a_0^{i+1} & a_1^{i+1} & a_2^{i+1} & a_3^{i+1} \end{bmatrix}^T \quad (4.15)$$

Then, the constraints (4.8), (4.11) and (4.14) can be written as:

$$\begin{bmatrix} 1 & \Delta_{t_i} & \Delta_{t_i}^2 & \Delta_{t_i}^3 & -1 & -\Delta_{t_i} & -\Delta_{t_i}^2 & -\Delta_{t_i}^3 \end{bmatrix} \lambda_{i,i+1} = 0 \quad (4.16)$$

$$\begin{bmatrix} 0 & 1 & 2\Delta_{t_i} & 3\Delta_{t_i}^2 & 0 & -1 & -2\Delta_{t_i} & -3\Delta_{t_i}^2 \end{bmatrix} \lambda_{i,i+1} = 0 \quad (4.17)$$

$$\begin{bmatrix} 0 & 0 & 2 & 6\Delta_{t_i} & 0 & 0 & -2 & -6\Delta_{t_i} \end{bmatrix} \lambda_{i,i+1} = 0 \quad (4.18)$$

The initial point continuity conditions ($P1, DP1, D^2P1$) are expressed using the

first parameters of λ , using the following expression:

$$\begin{bmatrix} 1 & \Delta_{t_0} & \Delta_{t_0}^2 & \Delta_{t_0}^3 & 0 & 0 & 0 & 0 \end{bmatrix} \lambda_{0,1} = P1 \quad (4.19)$$

$$\begin{bmatrix} 0 & 1 & 2\Delta_{t_0} & 3\Delta_{t_0}^2 & 0 & 0 & 0 & 0 \end{bmatrix} \lambda_{0,1} = DP1 \quad (4.20)$$

$$\begin{bmatrix} 0 & 0 & 2 & 6\Delta_{t_0} & 0 & 0 & 0 & 0 \end{bmatrix} \lambda_{0,1} = D^2P1 \quad (4.21)$$

Analogous formulation for the final point and its position, velocity and acceleration values $P2, DP2, D^2P2$ can be constructed.

$$\begin{bmatrix} 0 & 0 & 0 & 0 & 1 & \Delta_{t_N} & \Delta_{t_N}^2 & \Delta_{t_N}^3 \end{bmatrix} \lambda_{N-1,N} = P2 \quad (4.22)$$

$$\begin{bmatrix} 0 & 0 & 0 & 0 & 0 & 1 & 2\Delta_{t_N} & 3\Delta_{t_N}^2 \end{bmatrix} \lambda_{N-1,N} = DP2 \quad (4.23)$$

$$\begin{bmatrix} 0 & 0 & 0 & 0 & 0 & 0 & 2 & 6\Delta_{t_N} \end{bmatrix} \lambda_{N-1,N} = D^2P2 \quad (4.24)$$

All the constraints can be written in a single matrix, which is represented by the constraint matrix C .

$$C\lambda = d \quad (4.25)$$

where, d is the value that the equation must take in order to meet the constraint conditions, which can be $P1, DP1, D^2P1, P2, DP2, D^2P2$ or zero depending on the waypoint and the condition being enforced. Recall that λ is the collection of all the parameters, that is, $\lambda = [\lambda_0 \ \lambda_1 \ \dots \ \lambda_N]$

The cost function is constructed evaluating the splines at each waypoint:

$$S_i(t_i) = \begin{bmatrix} 1 & \Delta_{t_i} & \Delta_{t_i}^2 & \Delta_{t_i}^3 \end{bmatrix} \lambda_i = P_i \lambda_i \quad (4.26)$$

Then, all the values of the splines at the waypoints can be calculated in vector form using the following equation:

$$S = \text{Diag}_{i=0}^N [P_i] \lambda = P \lambda \quad (4.27)$$

Finally, the minimization problem can be formulated as:

$$\min \|P\lambda - Y\| \quad (4.28)$$

$$s.t. \quad C\lambda = d \quad (4.29)$$

where, Y is the desired set of points describing the reference trajectory, in particular for the thesis $Y = C2$. Note that the problem can be solved in real time applications given its convex form. Moreover, an analytic solution can be obtained that can be implemented on the microcomputer of the prosthetic device AMPRO II.

4.2 Analytical solution

Considering the problem expressed in the optimization:

$$\min \|P\lambda - Y\| \quad (4.30)$$

$$s.t. \quad C\lambda = d$$

It is possible to rewrite the optimization problem as:

$$\min \|P\lambda - Y\| = \min \lambda^T P^T P \lambda - 2Y^T P \lambda + Y^T Y \quad (4.31)$$

$$s.t. \quad C\lambda = d$$

Then, the lagrangian of the optimization problem can be expressed as:

$$L = \lambda^T P^T P \lambda - 2Y^T P \lambda + Y^T Y + \nu^T (C \lambda - d) \quad (4.32)$$

Using the KKT conditions for optimality:

$$2P^T P \lambda - 2P^T Y + C^T \nu = 0 \quad (4.33)$$

$$C \lambda = d \quad (4.34)$$

It represents a matricial linear equation on (λ, ν) that can be expressed as:

$$\begin{pmatrix} 2P^T P & C^T \\ C & 0 \end{pmatrix} \begin{pmatrix} \lambda \\ \nu \end{pmatrix} = \begin{pmatrix} 2P^T Y \\ d \end{pmatrix} \quad (4.35)$$

This equation can be solved for λ and ν easily using Eigen Libraries in C++, which can be implemented in real time and fits our requirements of implementation. An Eigen-based library has been created for the generation of a family of splines satisfying the conditions of smoothness and continuity. The public repository is located in: bitbucket.org/pvictorm6/splines_support

4.3 Human-inspired walking with cubic splines

The first connection between the set of cubic splines and the canonical walking functions is given by their parameterization in time. However, as mentioned earlier, a replacement of time is given by $\rho(\theta)$ in (3.15) which will be adopted by the splines as well. To fully define the domain of the splines, the boundary conditions must be explicitly stated, the splines will take action while $\rho(\theta) \in [t_s, t_s]$, otherwise, the canonical walking functions for flat ground walking will be used.

As soon as the prosthetic foot lands on a arbitrary surface, the values of its position, velocity and acceleration can be used for the boundary conditions of the initial point (P_1 , DP_1 , D^2P_1). Considering that the objective function is the connection of this point to its respective flat ground CWF, the final boundary conditions (P_2 , DP_2 , D^2P_2) are defined in terms of the desired values of the relative degree two canonical walking functions.

$$P_2 = y_2^d(\rho^*, \alpha) \quad (4.36)$$

$$DP_2 = \dot{y}_2^d(\rho^*, \alpha) \quad (4.37)$$

$$DDP_2 = \ddot{y}_2^d(\rho^*, \alpha) \quad (4.38)$$

where, $\rho^* = t_c + t_s$ is the designed convergence time which corresponds to the time when the splines smoothly intersects the CWF. Note that the evaluation of the spline will be computed from the following equation:

$$S(\rho(\theta)) = \begin{bmatrix} 1 & \rho(\theta) & \rho(\theta)^2 & \rho(\theta)^3 \end{bmatrix} \lambda_{i(\rho(\theta))} \quad (4.39)$$

where, $\lambda_{i(\rho(\theta))}$ is the set of spline parameters corresponding to $\rho(\theta)$. The relative degree two outputs will depend on the spline trajectory or the CWF. Therefore, the outputs can be expressed as:

$$y_2(\theta, \alpha) = \begin{cases} y_2^a(\theta) - S(\rho(\theta)), & if \quad \rho(\theta) \leq \rho^* \\ y_2^a(\theta) - y_2^d(\rho(\theta), \alpha), & if \quad \rho(\theta) > \rho^* \end{cases} \quad (4.40)$$

Note that using the spline formulation, we lose the guarantees about stability because the splines trajectories will evolve outside the PHZD surface. However,

since the human inherent controller is highly adaptable and robust we assume that the user will remain stable considering the small changes introduced by the spline. Furthermore, the trajectories generated by the use of splines will converge to the provably stable CWF.

4.3.1 Trajectories generated

Using the optimization problem proposed, a simulation in MATLAB was performed to obtain the resulting trajectories for ankle and knee under a different initial and final condition (4.4) based on the designed flat ground trajectories (Fig. 3.4). The optimization was solved using the analytical solution shown in (4.35). Note that both extremes are generated using the spline formulation for the estimation of the behavior of the joints. However, the implementation of the framework dictates that the first part the prosthetic standing phase is generated using the spline trajectory generation and the last part of the prosthetic swing phase is generated through the use of low gain PD control. The results achieved using the analytic form of the problem yields the same results as using the quadratic program solver built-in in MATLAB. This results were also tested in C++ for a series of different conditions to ensure that the solutions are valid.

4.4 Implementation details

The Table 4.1 shows the parameters used to generate the splines and activate the impedance control, note that the parameterized time indicates 100% of step progression. The low gain PD control is used on the final part of the prosthetic swing phase and is aimed to grant terrain adaptation and provide the initial conditions to the spline formulation. The controller can be expressed as:

$$u = K_p(\theta_d^i - \theta_a^i) + K_d(\dot{\theta}_d^i - \dot{\theta}_a^i), \quad i \in \{\text{ankle, knee}\} \quad (4.41)$$

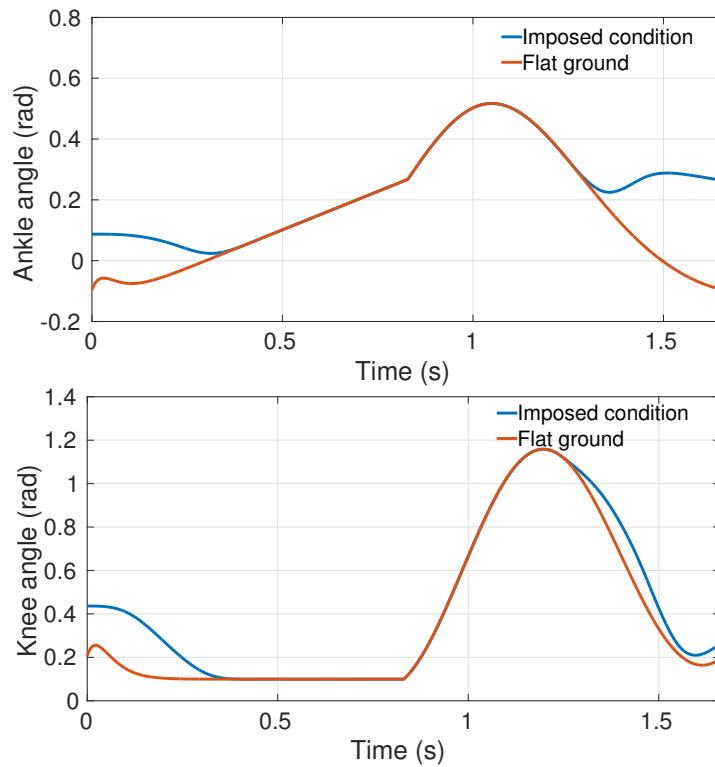


Figure 4.4: Trajectory generation for ankle and knee joint. The splines has been generated in two extremes to show the effect of the splines.

Table 4.1: Implementation parameters

Parameter	Value	Unit
<i>Switching time</i>	0	Unitless
<i>Convergence time</i>	0.2	Unitless
<i>Impedance time</i>	0.6	Unitless
<i>Parameterized time (max)</i>	0.823	Unitless

5. RESULTS

In order to verify the applicability of the algorithms proposed they were implemented in the transfemoral prosthesis AMPRO II. The experiments were performed by a healthy subject with a knee adapter [13] (Fig. 5.1) that allowed him to bend his human knee to use the transfemoral prosthesis simulating an amputation. Additionally, a comparison between Human-Inspired Control (HIC) and the Splines-based Human-Inspired Control (SHIC) is realized to motivate the usage of SHIC as a controller able to perform flat ground and upslope walking.

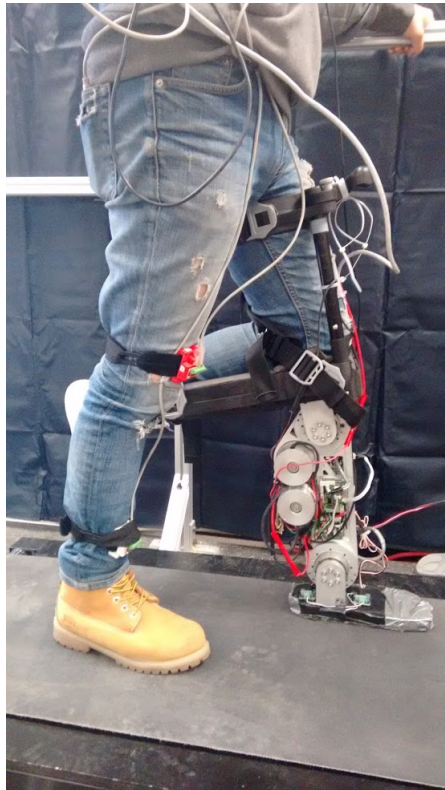


Figure 5.1: Healthy subject using a knee adapter to use the transfemoral prosthesis AMPRO II



Figure 5.2: Indoors flat ground walking experiment using SHIC.

The experiments were realized inside the laboratory space (Fig. 5.2) and outside of the laboratory (Fig. 5.3). Both experiments consisted in flat ground walking and upslope walking tests. The subject was asked to perform two trials: (1) to walk in straight line in a flat ground surface for 5 min, and (2) walk in flat ground terrain toward an slope and immediately transition into upslope walking without any stop procedure.

5.1 Flat ground walking

The spline-based controller is aimed to enable an upslope walking, however, it is expected to work even for flat ground terrain. In order to support this claim flat ground experiments were realized using HIC and SHIC under the same conditions and letting the human subject to use a self-paced speed. In both experiments, after some practice the user achieved to walk without holding the security handrails as



Figure 5.3: Outdoors experiment using SHIC.

seen in Fig. 5.10, which particularly corresponds to SHIC.

5.1.1 HIC results

HIC was used in the AMPRO II and provided stable walking for the subject, in particular, the trajectories achieved are shown in Fig. 5.4 for the ankle and knee respectively. Note that tracking is achieved throughout the trajectory.

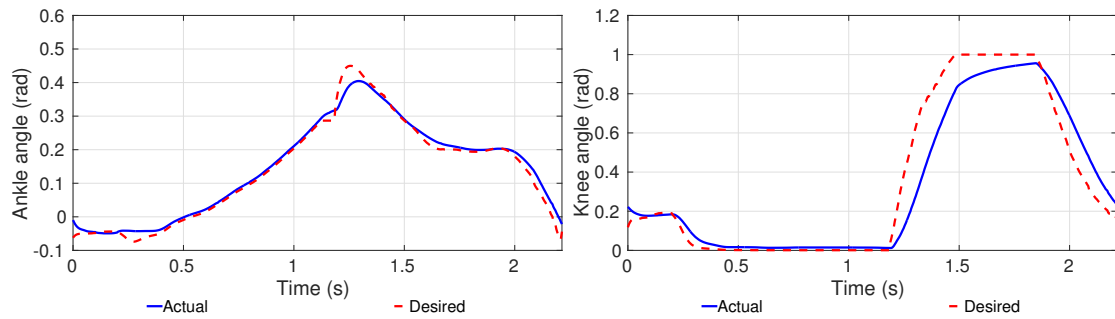


Figure 5.4: Ankle and knee Tracking for flat ground walking using HIC.

5.1.2 SHIC results

SHIC was used in AMPRO II, the experiments lead as well to stable walking. The trajectories achieved are shown in Fig. 5.5 for ankle and knee respectively. Note that tracking is lost in the final part of the step because of the low gain PD.

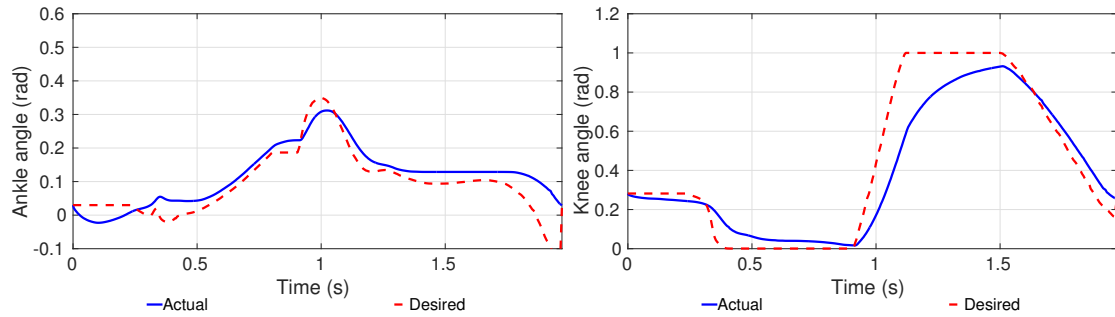


Figure 5.5: Ankle and knee Tracking for flat ground walking using SHIC.

5.2 Upslope walking

The main focus of the thesis is to show upslope walking capabilities in the trans-femoral prosthesis. The upslope walking data was captured during the indoors experiment (Fig. 5.11), were the subject performed several trials on the sloped surface. The inclination of the slope was 13° . Fig. 5.6 represents the trajectories of the ankle and knee respective.

5.3 Controllers comparison

Both controllers HIC and SHIC resulted in stable walking for flat ground walking, however they have some differences in the trajectories generated. Because of this, it is important to explain the differences in the controller action that leads to such differences. Additionally, a comparison between flat ground walking and upslope

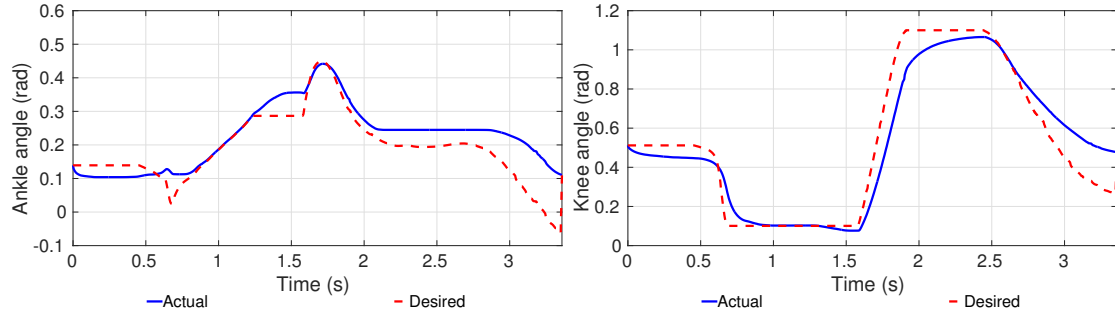


Figure 5.6: Upslope walking trajectories for ankle and knee. The slope inclination is 13° .

walking with SHIC is realized to observe the effect of the splines.

5.3.1 Flat ground walking using HIC and SHIC

Comparing the trajectories generated by the use of HIC and SHIC (Fig. 5.7) it can be noted that SHIC ankle suffers a deviation with respect to HIC, this is explained by the low gain PD algorithm which is used for terrain adaptation. The knee joints show a very similar evolution for both HIC and SHIC controllers. It is important to recall that both controllers lead to stable walking during the experiments. The SHIC experimental walking tiles can be seen in Fig. 5.10.

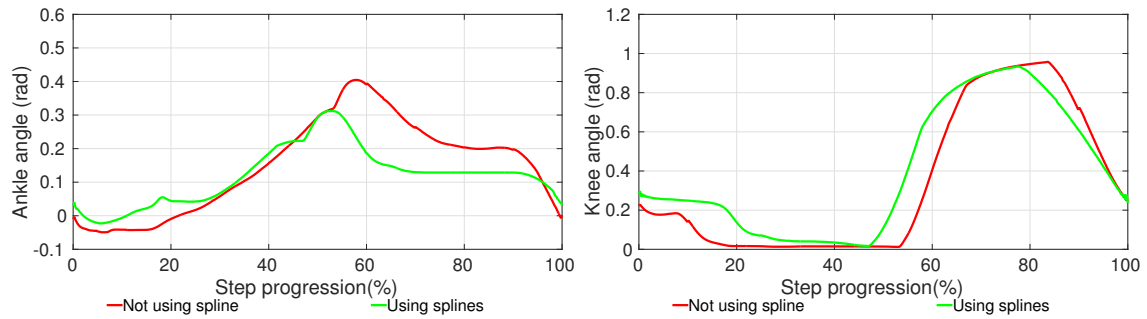


Figure 5.7: Superposition of the trajectories for flat ground surfaces using both controllers, splines-based human-inspired control and normal human-inspired control

5.3.2 Flat ground and upslope walking using SHIC

By exploring the differences in the trajectories obtained through the use of the splines-based controller is possible to visualize the effect of the SHICs and the verification of the strategies proposed to perform upslope walking. The ankle and knee trajectories are shown Fig. 5.8 for both terrains. It can be observed that the upslope ankle shows a small offset with respect to flat ground walking (3°), however knee presents the qualitative behavior expected: an increase on knee flexion to avoid foot scuffing and to mimic the human strategies for upslope walking. Note that the assumption of flat foot affects primarily the ankle behavior, the next step is the implementation of a multi-contact walking algorithm [31].

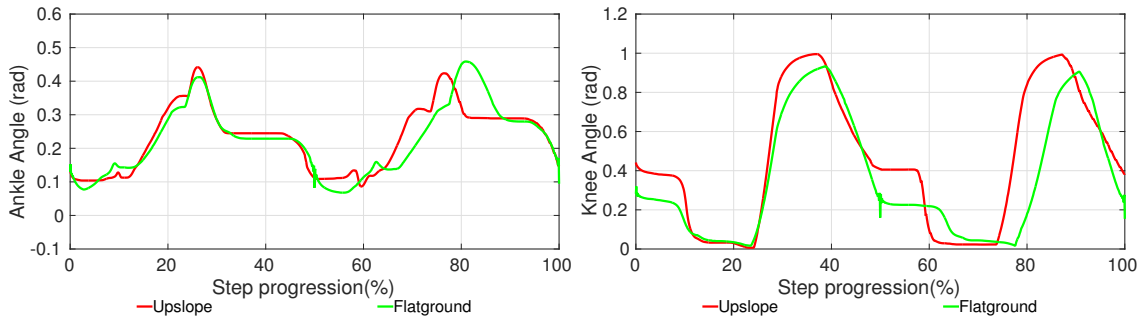


Figure 5.8: 2-steps trajectory differences between flat ground and upslope walking using SHIC.

5.4 SHIC control action

The control action of the SHIC can be observed by looking at the tracking plots, in particular Fig. 5.9 shows the regions of action of the low gain PD and the splines. In particular, the red shaded region corresponds to the action of the low gain PD, it is observed that in this region the tracking is lost in order to gain terrain adaptation.

The blue shaded regions corresponds to the action of the splines, which takes the actual value of the joints and blends the trajectory to perform upslope walking.

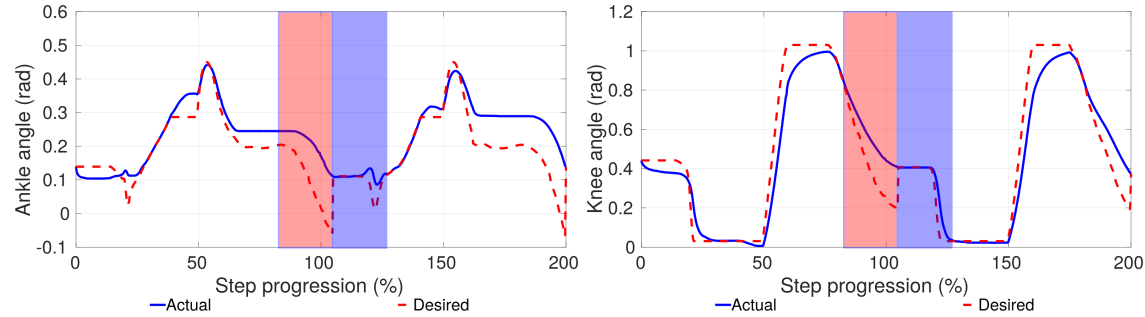


Figure 5.9: SHIC low gain PD (red region) and spline generation (blue region) for two steps.



Figure 5.10: Flat ground walking using SHiC.



Figure 5.11: Transition between flat ground walking to upslope walking using SHiC.



Figure 5.12: Upslope walking sequence using SHIC.

6. CONCLUSIONS

The insertion of the proposed algorithm successfully reproduced the strategy of healthy humans when they perform upslope walking, leading the human subject to perform upslope walking with the prosthetic device AMPRO II. The tiles (Fig. 5.10, Fig. 5.11 and Fig. 5.12) show that the same control algorithm can be used to generate flat ground and upslope walking gaits within the same framework. In fact, the comparison made for flat ground walking using both controllers yielded similar results for ankle and knee (Fig. 5.4) which motivates the use of the SHIC for the generation of gaits for flat ground and upslope walking.

During upslope walking the knee trajectory generated by the use of splines and impedance control is consistent with the strategy found during healthy human walking in inclined surfaces [16, 14, 12], furthermore, the changes in knee are correlated to the human knee sensitivity with respect to the slope inclination [16].

The thesis proposed successfully a control framework based on the use of a set of cubic-splines based on an optimization problem and low gain PD control for performing upslope walking. The control framework blends the joint trajectories from flat ground walking into upslope walking. Furthermore, the controller automatically generates walking gaits for flat ground and upslope walking without large tuning requirements.

Future research needs to be focused on the use of multi-contact walking gaits with the set of cubic splines proposed. Additionally, entire trajectories could be generated using an appropriate optimization formulation.

REFERENCES

- [1] Aaron D. Ames. First steps toward automatically generating bipedal walking from human data. *Robot Motion and Control 2011*, Springer London:89–116, 2012.
- [2] Aaron D. Ames. Human-inspired control of bipedal walking robots. *IEEE Transactions on Automatic Control.*, 59(5), 2014.
- [3] B Cao, GI Dodds, and GW Irwin. Constrained time-efficient and smooth cubic spline trajectory generation for industrial robots. In *Control Theory and Applications, IEE Proceedings-*, volume 144, pages 467–475. IET, 1997.
- [4] Rafal Goebel, Ricardo G Sanfelice, and Andrew Teel. Hybrid dynamical systems. *Control Systems, IEEE*, 29(2):28–93, 2009.
- [5] Robert D Gregg and Jonathon W Sensinger. Towards biomimetic virtual constraint control of a powered prosthetic leg. *Control Systems Technology, IEEE Transactions on*, 22(1):246–254, 2014.
- [6] A Hereid, S. Kolathaya, M.S Jones, Van Why J.W, and A. D. Ames. Dynamic multi-domain bipedal walking with atrias through slip based human-inspired control. In ACM, editor, *Proceedings of the 17th International conference on Hybrid systems: computation and control.*, 2014.
- [7] Ayonga Hereid, Christian M Hubicki, Eric A Cousineau, Jonathan W Hurst, and Aaron D Ames. Hybrid zero dynamics based multiple shooting optimization with applications to robotic walking. In *Robotics and Automation (ICRA), 2015 IEEE International Conference on*, pages 5734–5740. IEEE, 2015.

- [8] Neville Hogan. Impedance control: An approach to manipulation: Part iiimplementation. *Journal of dynamic systems, measurement, and control*, 107(1):8–16, 1985.
- [9] Shishir Kolathaya and Aaron D Ames. Achieving bipedal locomotion on rough terrain through human-inspired control. In *Safety, Security, and Rescue Robotics (SSRR), 2012 IEEE International Symposium on*, pages 1–6. IEEE, 2012.
- [10] J. Zico Kolter and Andrew Y. Ng. Task-space trajectories via cubic spline optimization. In *Robotics and Automation, 2009. ICRA '09. IEEE International Conference on*, pages 1675–1682, 2009.
- [11] Brian Edward Lawson, J Mitchell, Don Truex, Amanda Shultz, Elissa Ledoux, and Michael Goldfarb. A robotic leg prosthesis: Design, control, and implementation. *Robotics & Automation Magazine, IEEE*, 21(4):70–81, 2014.
- [12] Andrea N. Lay, Chris J. Hass, and Robert J. Gregor. The effects of sloped surfaces on locomotion: A kinematic and kinetic analysis. *Journal of Biomechanics*, 39:1621–1628, 2006.
- [13] Edward D Lemaire, David Nielen, and Marie Andrée Paquin. Gait evaluation of a transfemoral prosthetic simulator. *Archives of physical medicine and rehabilitation*, 81(6):840–843, 2000.
- [14] Alain Leroux, Joyce Fung, and Hugues Barbeau. Postural adaptation to walking on inclined surfaces: I. normal strategies. *Gait & posture*, 15(1):64–74, 2002.
- [15] Owings Maria F. and Kozak Lola Jean. Ambulatory and inpatient procedures in the united states, 1996. *National Center for Health Statistics.*, Vital Health(Stat 13(139)), 1998.

- [16] Andrew Stuart McIntosh, Karen T. Beatty, Leanne N. Dwan, and Deborah R. Vickers. Gait dynamics on an inclined walkway. *Journal of Biomechanics*., 39(13):2491–2502, 2006.
- [17] Craig D Murray. The social meanings of prosthesis use. *Journal of Health Psychology*, 10(3):425–441, 2005.
- [18] T.S. Parker and L.O. Chua. *Practical numerical algorithms for chaotic systems*. Springer New York, 1989.
- [19] Shankar. Sastry. *Nonlinear systems: analysis, stability, and control.*, volume 10. Springer Science & Business Media, 2013.
- [20] Ryan W. Sinnet, Matthew J. Powell, Rajiv P. Shah, and Aaron D. Ames. A human-inspired hybrid control approach to bipedal robotic walking. In *18th IFAC World Congress*, 2011.
- [21] Douglas G. Smith. The transfemoral amputation level, part 1. URL: "<http://www.amputee-coalition.org/resources/transfemoral-amputation-part-1/>", Accessed: 03/01/2016.
- [22] Frank Sup, Amit Bohara, and Michael Goldfarb. Design and control of a powered transfemoral prosthesis. *The International Journal of Robotics research*., 27(2):263–273, 2008.
- [23] Frank Sup, Huseyin Atakan Varol, and Michael Goldfarb. Upslope walking with a powered knee and ankle prosthesis: initial results with an amputee subject. *Neural Systems and Rehabilitation Engineering, IEEE Transactions on*., 19(1):71–78, 2011.
- [24] RL Waters, J Perry, D Antonelli, and H Hislop. Energy cost of walking of amputees: the influence of level of amputation. *The Journal of bone and joint*

- surgery.*, 1(58):42–46, 1976.
- [25] Eric DB Wendel and Aaron D. Ames. Rank properties of poincare maps for hybrid systems with applications to bipedal walking. In ACM, editor, *Proceedings of the 13th ACM international conference on Hybrid systems: computation and control.*, 2010.
 - [26] E. R Westervelt, J. W. Grizzle, C Chevallereau, J Choi, and B. Morris. *Feedback control of dynamic bipedal robot locomotion*. CRC press, 2007.
 - [27] E.R Westervelt, J.W Grizzle, and Koditscheck. D.E. Hybrid zero dynamics of planar biped walkers. *IEEE Transactions on Automatic Control*, 48(1):42–56, 2003.
 - [28] Shishir Nadubettu Yadukumar, Murali Pasupuleti, and Aaron D. Ames. From formal methods to algorithmic implementation of human inspired control on bipedal robots. In Springer Berlin Heidelberg, editor, *Algorithm Foundations of human inspired control on bipedal robots.*, pages 511–526, 2013.
 - [29] H. Zhao, J. Reher, J. Horn, V. Paredes, and A. D. Ames. Realization of stair ascent and motion transitions on prostheses utilizing optimization-based control and intent recognition. In IEEE, editor, *Rehabilitation Robotics (ICORR), 2015 IEEE International Conference on.*, 2015.
 - [30] Hui-Hua Zhao, WL Ma, Zeagler MB, and A. D. Ames. Human-inspired multi-contact locomotion with amber2. *ACM/IEEE 5th International Conference on Cyber-Physical Systems (with CPS Week 2014)*, IEEE Computer Society, 2014.
 - [31] Huihua Zhao, Jonathan Horn, Jacob Reher, Victor Paredes, and Aaron D Ames. Multi-contact locomotion on transfemoral prostheses via hybrid system models and optimization-based control.

- [32] Huihua Zhao, M. J. Powell, and A. D. Ames. *Optimal Control Applications and Methods*, chapter Human-inspired motion primitives and transitions for bipedal robotic locomotion in diverse terrain., pages 730–755. 2014.
- [33] Huihua Zhao, Jake Reher, Jonathan Horn, Victor Paredes, and Aaron D. Ames. Realization of nonlinear real-time optimization based controllers on self-contained transfemoral prosthesis. In ACM, editor, *Proceedings of the ACM/IEEE Sixth International Conference on Cyber-Physical Systems.*, 2015.